Tracing the migration of mantle CO_2 in gas fields and mineral water springs in south-east Australia using noble gas and stable isotopes

Rūta Karolytė[1a*], Gareth Johnson[1], Domokos Györe[2], Sascha Serno[1], Stephanie Flude[1], Finlay M. Stuart[2], Allan R. Chivas[3,4], Adrian Boyce[2] and Stuart M.V. Gilfillan[1]

[1] School of GeoSciences, University of Edinburgh, James Hutton Road, Edinburgh, EH9 3FE, UK

[2]Isotope Geoscience Unit, Scottish Universities Environmental Research Centre (SUERC), East Kilbride, G75 0QF, UK

[3]GeoQuEST Research Centre, School of Earth, Atmospheric and Life Sciences, University of Wollongong, Wollongong, NSW 2522, Australia

[4]Department of Earth Sciences and Sprigg Geobiology Centre, The University of Adelaide SA 5005, Australia

[a]Current address: Department of Earth Sciences, University of Oxford, 3 S Parks Rd, Oxford OX1 3AN, UK

*Author for correspondence: ruta.karolyte@earth.ox.ac.uk

Keywords: Carbon Capture and Storage; geochemical tracing; noble gases; carbon isotopes; helium; mantle; CO_2 springs; solubility fractionation; Otway Basin.

Abstract

Geochemical monitoring of CO_2 storage requires understanding of both innate and introduced fluids in the crust as well as the subsurface processes that can change the geochemical fingerprint of CO_2 during injection, storage and any subsequent migration. Here, we analyse a natural analogue of CO_2 storage, migration and leakage to the atmosphere, using noble gas and stable isotopes to constrain the effect of these processes on the geochemical fingerprint of the CO_2. We present the most comprehensive evidence to date for mantle-sourced CO_2 in south-east Australia, including well gas and CO_2-rich mineral spring samples from the Otway Basin and Central Victorian Highlands (CVH). $^3He/^4He$ ratios in well gases and CO_2 springs range from 1.21 to 3.07 R_A and 1.23 – 3.65 R_C/R_A, respectively. We present chemical fractionation models to explain the observed range of $^3He/^4He$ ratios, He, Ne, Ar, Kr, Xe concentrations and $\delta^{13}C(CO_2)$ values in the springs and the well gases. The variability of $^3He/^4He$ in the well gases is controlled by the gas residence time in the reservoir and

associated radiogenic ^{4}He accumulation. $^{3}He/^{4}He$ in CO_2 springs decrease away from the main mantle fluid supply conduit. We identify one main pathway for CO_2 supply to the surface in the CVH, located near a major fault zone. Solubility fractionation during phase separation is proposed to explain the range in noble gas concentrations and $\delta^{13}C(CO_2)$ values measured in the mineral spring samples. This process is also responsible for low ^{3}He concentrations and associated high $CO_2/^{3}He$, which are commonly interpreted as evidence for mixing with crustal CO_2. The elevated $CO_2/^{3}He$ can be explained solely by solubility fractionation without the need to invoke other CO_2 sources. The noble gases in the springs and well gases can be traced back to a single end-member which has suffered varying degrees of radiogenic helium accumulation and late stage degassing. This work shows that combined stable and noble gas isotopes in natural gases provide a robust tool for identifying the migration of injected CO_2 to the shallow subsurface.

1. Introduction

The development of geochemical tracing techniques to ascertain the origin and genetic link between natural gases trapped in subsurface reservoirs and those degassing at the surface is important to the safe and successful deployment of carbon capture and storage (CCS). Safe disposal of captured industrial CO_2 requires verification of the fate of the injected gas and reassurance that injected gas does not migrate to the surface (IPCC, 2005). To ensure this, CCS operators have to adhere to legislative guidelines and verify that injected CO_2 is securely contained within the reservoir formation (Dixon et al., 2015). While a variety of geophysical, geoelectric and thermal sensing monitoring techniques exist (Giese et al., 2009), the high sensitivity of geochemical monitoring techniques is useful for detecting seepage at low concentrations, verifying gas origin and tracing the interactions between different crustal fluids (Myers et al., 2013; Stalker and Myers, 2014; Roberts et al., 2017).

The noble gas isotopes have previously been applied in an engineered setting to assess CO_2 migration, dissolution and residual trapping in reservoir pore spaces at the Cranfield CO_2-EOR site field (Györe et al., 2015; Györe et al., 2017) and to study industrial underground natural gas storage in the Paris Basin (Jeandel et al., 2010). Noble gas tracers have been used to refute allegations of injected CO_2 leakage to the surface near the Weyburn-Midale CO_2 Monitoring and Storage Project (Gilfillan et al., 2017) and to identify fugitive gas migration to shallow aquifers caused by industrial hydraulic fracturing operations (Darrah et al., 2014). The techniques used in these industrial studies have been informed by preceding research of natural gas fields and springs (e.g. Ballentine and

61 O'Nions, 1994; Gilfillan et al., 2014, 2009, 2008; Sherwood Lollar et al., 1997; Wilkinson et al., 2009).
62 Natural analogue studies remain a crucial gateway to developing geochemical tracing methods for
63 the industrial sector, providing information about fluid migration and retention processes occurring
64 over geological time scales (Baines and Worden, 2004; Haszeldine et al., 2005; Holland and Gilfillan,
65 2013).

66 Helium is an unrivalled indicator of crustal fluid migration in the subsurface because it is
67 sensitive to changes in the balance between volatiles derived from the mantle and the crust. This is
68 because the original helium composition of any subsurface fluid is not significantly modified by
69 interaction with groundwater due to the low abundance of helium in the atmosphere (Ozima and
70 Podosek, 2002). Hence, helium is particularly applicable to tracing gas migration through a water
71 system in both natural and industrial fugitive gas migration monitoring settings. Here we draw from
72 existing methodologies of helium use in tracing the migration of mantle fluids (Sano et al., 1990;
73 Sakamoto et al., 1992), mixing of different fluid sources (O'Nions and Oxburgh, 1988; Sano and
74 Marty, 1995) and dating natural gas and groundwater resources (Zhou and Ballentine, 2006; Liu et
75 al., 2016) to provide a comprehensive account on the geochemical link between natural CO_2 gases,
76 trapped in the subsurface and emanating in the shallow surface.

77 Noble gases are soluble in water and partition according to their relative solubilities during
78 gas-water equilibration. This property has been utilised mainly in assessing reservoir-scale water-gas
79 equilibration and gas migration or groundwater recharge conditions (Bosch and Mazor, 1988;
80 Ballentine et al., 1996; Barry et al., 2016) and the presence of 'excess air' above the atmospheric
81 solubility equilibrium (Aeschbach-Hertig et al., 2008; Kipfer et al., 2002). The former is largely based
82 on atmospheric noble gas ratios, whilst the latter combines ratios with elemental concentrations.
83 Atmospheric noble gas ratios in CO_2 springs are commonly similar to air saturated-water (ASW) and
84 the utility of these noble gases is commonly overlooked. We discuss the use of noble gas
85 concentration data in assessing the solubility fractionation effects of near-surface degassing and
86 reconstructing the original noble gas composition for the purpose of tracing.

87 The physical and chemical processes contributing to and modifying the noble gas contents of
88 CO_2 are explored using the data from three natural CO_2 fields in the Otway Basin of SE Australia and
89 ten natural CO_2-rich springs in Victoria. We focus on identifying the origin of the gases and the
90 genetic link between gases stored in reservoir traps and those emanating at the surface from the
91 natural mineral springs.

92 # 2 Geological setting

93 ## 2.1 Basin setting and location of CO_2 gas fields and springs

94 The Otway Basin developed along the southern Australian margin as a result of crustal
95 extension due to sea floor spreading between Australia and Antarctica. The sedimentary section of
96 the basin comprises Upper Jurassic – Lower Cretaceous Otway Group sediments (Bernecker and
97 Moore, 2003). The present geometry of the basin is characterised by NW-SE trending normal faults,
98 and was established during Jurassic to Cretaceous rifting and subsequent reactivation during a short-
99 lived period of basin inversion in the Miocene (Cox et al., 1995; Teasdale et al., 2003).

100 The basement comprises Lachlan and Delamerian fold belts, separated by the Moyston
101 lithospheric suture which extends to the Moho (Fig. 1a). Parallel N-S trending large-scale shear zones
102 and reverse faults connect to the Moyston Fault at depth (Fig. 1d) (Cayley et al., 2011). The structure
103 of the Otway Basin has been strongly controlled by the fabric of the underlying basement. Old
104 basement structures have a significant rheology contrast along them and are more likely to undergo
105 structural reactivation during a change in the stress regime (Hand and Sandiford, 1999). The Jurassic-
106 Cretaceous extension was mainly accommodated along structural weaknesses of the basement,
107 which created graben and half-graben structures favourable for fluid trapping. Hydrocarbons and
108 CO_2 discoveries in the Otway Basin therefore tend to coincide with the location of deep basement
109 faults (Bernecker and Moore, 2003).

110 The basin contains numerous accumulations of CO_2, methane and other hydrocarbons in
111 varying concentrations (Boult et al., 2004). The three gas fields investigated in this work contain CO_2
112 concentrations above 75 mol %, with the remainder of the gas content being primarily methane. The
113 Caroline field is located in South Australia, near Mt Gambier and is a commercially explored CO_2 field
114 which has a CO_2 concentration in excess of 98 %. At reservoir depth and temperature (2.5 km, 92 °C),
115 CO_2 is in a supercritical fluid phase (Chivas et al., 1987). Boggy Creek and Buttress fields are located
116 in the Port Campbell Embayment at the eastern side of the Otway Basin. Both fields contain
117 mixtures of CO_2 and methane in the gas phase with no significant liquid hydrocarbon component
118 (Boreham et al., 2011). Methane generation is dated to mid-Paleogene (Duddy, 1997), followed by a
119 later-stage CO_2 emplacement (Boult et al., 2004; Watson et al., 2004; Lyon et al., 2005).

120 CO_2-rich mineral spring waters emanate at the ground surface within the extent and north of
121 the basin. Over a hundred ambient temperature mineral springs are located in the Central Victorian
122 Highlands (CVH) (Fig. 1b). Mineral water flows through a fracture-dominated aquifer consisting of
123 Ordovician low-grade metasedimentary sequence and discharges into topographic lows such as

streambeds. Many of the springs also release CO_2 and can be identified as degassing CO_2 bubble trails into creek beds or standing pools of water. Springs are clustered along the Muckleford Fault, which is a deep Proterozoic reverse fault extending down to the lower crust and connecting to the Moyston suture zone (Cayley et al., 2011) (Fig. 1d).

Mineral springs also emerge on the northern coast of Bellarine Peninsula, at Clifton Springs near Geelong, on the south-eastern edge of the Otway Basin (Fig. 1c). The central part of the Bellarine Peninsula has been uplifted in the late Miocene during the inversion of NE-SW trending normal faults (Coulson, 1933). The north coast of the peninsula is structurally controlled by the Curlewis Monocline, underlain by a south dipping normal fault. The Curlewis Monocline is parallel to the structural lineaments of the basement and could be associated with deeper basement faults (Dahlhaus, 2003). CO_2 springs emerge along the shoreline parallel to the fault.

The basement and the Otway Basin are overlain by the Newer Volcanic Province (NVP) extrusives that stretch from the CVH to the northern edges of the Port Campbell Embayment. The province is a well preserved intra-plate basaltic lava field with more than 400 eruptive centres (Boyce, 2013), active between 5 Ma and 4.5 ka (Cas et al., 2017). The last eruption dated at 4.5 ka, occurred at Mount Gambier, located near the Caroline CO_2 field (Robertson et al., 1996). Many of the oldest eruptive centres are found in the eastern side of the province and near the CVH (4.6 - 2.6 Ma) (Price et al., 1997), but no systematic pattern of eruption ages exists (Cas et al., 2017). There is no evidence for volcanic activity of this period in the Bellarine Peninsula where Clifton Springs are located, although The Older Volcanics (39 - 49 Ma) crop out in the area (Price et al., 1997). The cause of the recent volcanism is currently unresolved. Common theories include a mantle plume (Wellman and McDougall, 1974; Wellman, 1983), edge-driven isolated mantle convection (King and Anderson, 1998), batch-melting caused by fault reactivation (Lesti et al., 2008), or a combination of all these factors (Demidjuk et al., 2007; Davies and Rawlinson, 2014).

2.2 Previous noble gas studies of the gas fields and CO_2 springs

Despite the commercial exploration of CO_2 gas fields in the Otway Basin and springs in the CVH, studies of the CO_2 origins have been limited and the processes associated with the gas migration in the subsurface and to the surface are poorly understood. MORB and solar noble gas signatures have been identified in mantle xenolith samples from the Newer Volcanics (Matsumoto et al., 1997, 2002), primarily within CO_2-rich fluid inclusions (Matsumoto et al., 1998). Chivas et al. (1987) reported $^3He/^4He$ values of up to 3.1 R_A in the Caroline field and Caffee et al. (1999) identified the presence of primordial Xe in the field, providing evidence for a mantle source. Mantle helium has

also been reported in the Lavers-1 gas field in the Otway Basin (1.68 R/R_A) (Watson et al., 2004). Preliminary $^3He/^4He$ measurements of up to 3.1 R_A have been reported in CO_2 springs at the CVH (Chivas et al., 1983) but no further study has been published. It has been suggested that the source of mantle volatiles in CO_2 springs is associated with the NVP (Lawrence, 1969), however no conclusive evidence currently exists other than geographic proximity to the eruptive centres. Prior to this work no geochemical study into the origin of the CO_2 degassing at the Bellarine Peninsula had been published.

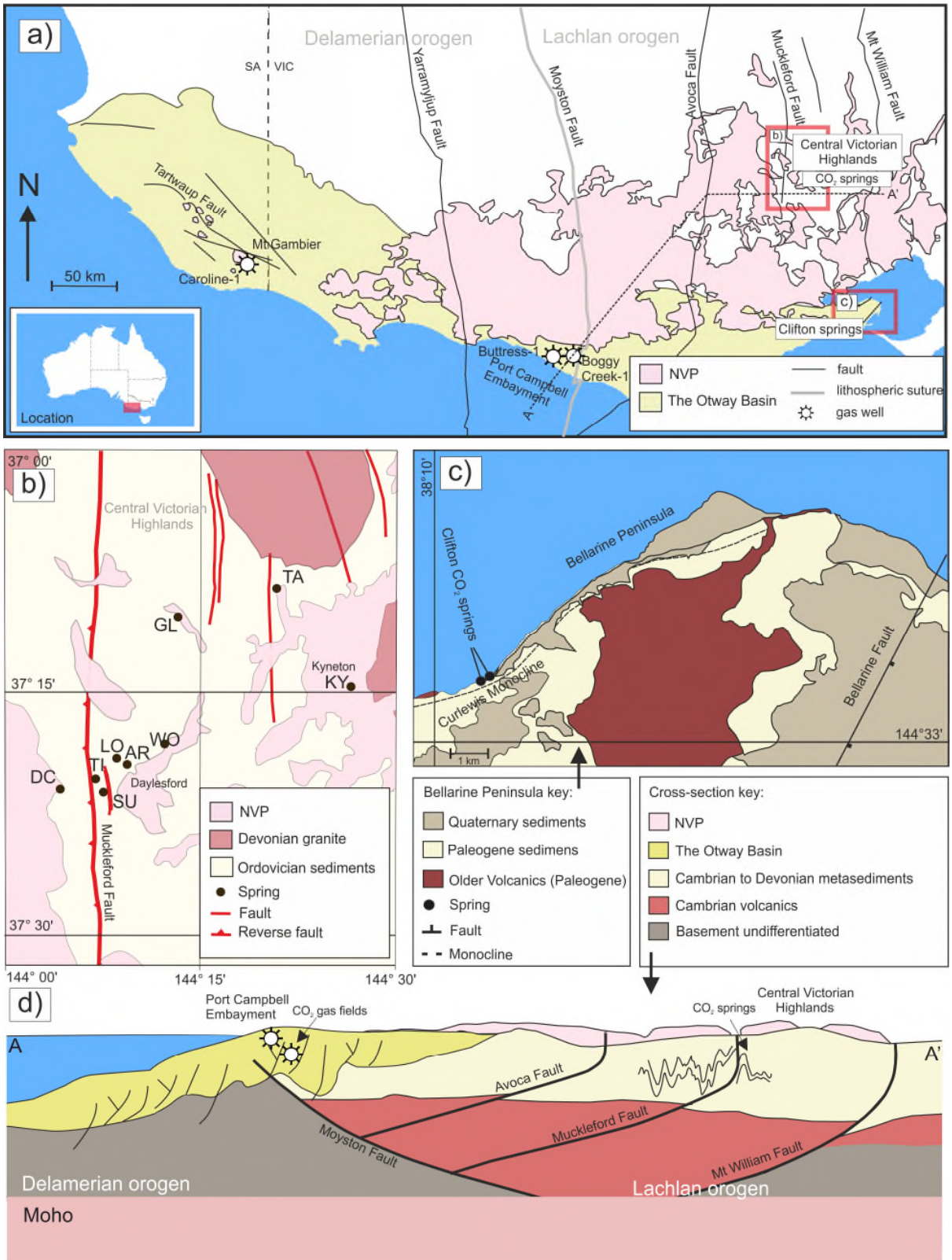

Figure 1. Location map of the studied CO_2 gas fields and springs. a) Studied well gases are in two localities in the Otway Basin: Port Campbell Embayment and Mt Gambier. Clifton Springs are located on the eastern edge of the basin. The CVH CO_2 springs emerge from the Ordovician basement rocks in the CVH (Central Victorian Highlands). The Otway Basin and CVH are dissected by N-S trending faults. The NVP (Newer Volcanic Province) extends across both areas. b) Location of sampled CO_2 springs in CVH; many of the springs are located near the Muckleford Fault (see Table 1 for sample name abbreviations). c) Clifton Springs are located on the coast of Bellarine Peninsula, along the crest of the Curlewis

Monocline. d) Sketch cross-section (not to scale) of A-A' transect on Fig. 1a, showing the structural relationship between the basement and the basin. The Moyston and Mt Williams Faults extend to the Moho. Many of the basement faults (including The Muckelford fault at CVH) are inferred to be connected to the Moyston Fault at depth. Elements of the figure adapted from (Cartwright et al., 2002; Bernecker and Moore, 2003; Watson et al., 2003; Cayley et al., 2011; Cas et al., 2017).

2. Methods

2.1 Gas sampling

The reported samples are in two distinct groups: 'well samples' refer to produced gases collected from well heads. 'Spring samples' refer to sample collected at water pools and streams where CO_2 is naturally degassing. Gas samples from the natural gas fields in the Otway Basin were collected directly from producing well heads, using 9.5 mm diameter refrigeration grade copper tubing connected to a pressure regulator by plastic hosing. Bubbling gases from the springs were collected using an inverted plastic funnel placed over a bubbling vent, placed into the water column to form an air-tight seal, allowing gas to flow through plastic hose to the copper tube. Tubes were purged for 5 minutes and sealed using two steel clamps specifically manufactured for the purpose of creating a helium leak-tight cold weld seal (Holland and Gilfillan, 2013). Mineral spring water samples were collected via hand pumps, filtered through 0.45 μm pore-size filters and filled into Nalgene bottles. The temperature, pH and TDS of the water in shallow tube bores was measured in the field using a Hanna Instruments HI991300 Portable Waterproof temperature/pH/EC Meter with an accuracy of ± 0.5 °C, ± 0.01 pH and ± 1 μS/cm for temperature, pH and electrical conductivity respectively. TDS values were obtained from EC measurements using a conversion factor of 0.7 (Walton, 1989).

2.2 Laboratory procedures

All laboratory work was undertaken at the Scottish Universities Environmental Research Centre (SUERC). Copper tube samples were connected to an all-metal vacuum line, purified using VG Scienta ST22 titanium sublimation pump and ZrAl alloy getter. The isotopic composition of noble gases was measured using a MAP 215-50 mass spectrometer using techniques outlined in Györe et al. (2015). Bulk gas concentrations were measured using a Pfeiffer Vacuum QMS 200 quadrupole mass spectrometer and Hewlett Packard 5890 Series 11 Gas Chromatograph with uncertainties of ±1 %. Major gas concentrations are reported corrected for air. $\delta^{13}(CO_2)$ values were determined using a VG Optima dual inlet isotope ratios mass spectrometer in dynamic mode using an internal standard (Dunbar et al., 2016). Values are reported relative to VPDB standard with uncertainties of ±0.2 ‰.

3. Results

A total of three well gas and ten spring samples were measured. Sample location, bulk gas composition, $\delta^{13}(CO_2)$ values, temperature, pH and TDS measurements are reported in Table 1. He, Ne and Ar isotope ratios, and He, Ne, Ar, Kr, Xe concentrations are reported in Table 2. The full suite of noble gases was measured in six of the CO_2 spring samples, while only He and Ne isotopes were measured in three well gas and four CO_2 spring samples.

Table 1. Details of the geographic location, bulk gas composition, $\delta^{13}(CO_2)$ values of 3 well gases and 10 CO_2 springs; pH, temperature and TDS measured in water from 10 mineral water bores.

Sample name	Label	Location			Bulk gas composition*						$\delta^{13}C(CO_2)$	Water from shallow bores		
		Region	Latitude	Longitude	CO_2	CH_4	C_2H_6	C_3H_8	C_4H_{10}	N_2	VPDB	pH	T °C	TDS g/L
Well gases														
Caroline-1	**CA**	Mount Gambier, SA	-37.9417	140.9083	99	0.9	0.01	–	–	0.4	-4.1	–	–	–
Boggy Creek-1	**BC**	Port Campbell, VIC	-38.5261	142.8245	87	10.0	0.1	0.03	0.01	2.3	-5.6	–	–	–
Buttress-1	**BU**	Port Campbell, VIC	-38.5167	142.8084	77	19.7	0.8	1.1	–	1.9	-7.6	–	–	–
CO_2 springs														
Taradale	**TA**	CVH	-37.1393	144.3500	>99						-9.4	6.1	20.9	2.9
Locarno	**LO**	CVH	-37.3113	144.1412	>99						-7.2	6.1	16.7	1.6
Deep Creek	**DC**	CVH	-37.3419	144.0733	>99						-8.2	5.6	15.7	0.6
Glenluce	**GL**	CVH	-37.1623	144.2225	>99	0.1					-7.8	6.3	16.7	2.2
Woolnoughs	**WO**	CVH	-37.2942	144.2065	>99						-6.9	6.2	21.1	1.6
Clifton Springs	**CS**	Bellarine Peninsula	-38.1510	144.5659	>99						-6.0	5.5	20.5	3.8
Sutton	**SU**	CVH	-37.3480	144.1317	>99						-8.4	6.0	19.7	1.1
Argyle	**AR**	CVH	-37.3141	144.1553	>99						-9.2	5.8	15.1	1.0
Kyneton	**KY**	CVH	-37.2358	144.4200	>99						-8.0[a]	6.1	18.3	1.2
Tipperary	**TI**	CVH	-37.3391	144.1186	>99						-7.1	6.3	16.5	2.2

* Bulk gas composition for Caroline-1 from Chivas et al. (1987), Boggy Creek-1 from Akbari (1992)

[a] from Cartwright et al. (2002)

212 **Table 2. Noble gas concentrations and isotopic ratios for 3 well gas samples and 10 CO_2 springs.**

Sample name	$^{3}He/^{4}He$ (R_C/R_A)		$^{20}Ne/^{22}Ne$		$^{21}Ne/^{22}Ne$		$^{40}Ar/^{36}Ar$		$^{38}Ar/^{36}Ar$		$^{4}He \times 10^{-6}$		$^{20}Ne \times 10^{-9}$		$^{40}Ar \times 10^{-5}$		$^{84}Kr \times 10^{-9}$		$^{132}Xe \times 10^{-10}$	
Well gases																				
Caroline-1	3.07	(0.12)	–		–		–		–		96.0	(5.0)	2.2	(0.1)	–		–		–	
Boggy Creek-1	1.21	(0.01)	–		–		–		–		384.4	(18.6)	124.1	(5.3)	–		–		–	
Buttress-1	1.25	(0.01)	–		–		–		–		478.8	(23.2)	15.4	(0.7)	–		–		–	
CO_2 springs																				
Taradale	1.23	(0.03)	9.73	(0.06)	0.030	(0.001)	314	(1)	0.195	(0.008)	4.0	(0.2)	34.3	(1.5)	5.3	(0.2)	8.2	(0.3)	6.9	(0.4)
Locarno	3.14	(0.09)	9.68	(0.05)	0.030	(0.001)	303	(1)	0.191	(0.003)	5.7	(0.2)	59.1	(2.5)	7.8	(0.3)	10.4	(0.43)	6.5	(0.3)
Deep Creek	2.45	(0.07)	9.92	(0.05)	0.029	(0.001)	301	(5)	0.190	(0.003)	8.9	(0.4)	132.3	(5.6)	22.8	(0.8)	39.5	(1.6)	30.4	(1.6)
Glenluce	1.57	(0.07)	9.71	(0.05)	0.028	(0.000)	308	(1)	0.189	(0.003)	163.0	(6.0)	1372	(58)	94.4	(3.5)	63.1	(2.6)	25.6	(1.3)
Woolnoughs	1.71	(0.07)	9.78	(0.06)	0.030	(0.001)	299	(1)	0.190	(0.003)	0.97	(0.04)	1781	(3.7)	86.0	(3.2)	79.9	(3.3)	36.1	(1.9)
Clifton Springs	1.97	(0.06)	9.73	(0.06)	0.029	(0.001)	323	(1)	0.191	(0.003)	42.0	(2.0)	128.8	(5.5)	22.9	(0.8)	29.8	(1.2)	19.9	(1.0)
Sutton	3.14	(0.03)	–		–		–		–		1.61	(0.05)	42.5	(1.5)	–		–		–	
Argyle	3.65	(0.08)	–		–		–		–		87.9	(2.6)	5502	(196)	–		–		–	
Kyneton	1.24*	(0.04)	–		–		–		–		4.9	(0.1)	13834	(493)	–		–		–	
Tipperary	2.70	(0.05)	–		–		–		–		0.48	(0.01)	438.3	(8.9)	–		–		–	

213 Concentrations are in $cm^3(STP)/cm^3$. Standard conditions are 0 °C at 1 bar.

214 Errors are 1σ standard deviation.

215 * $^{3}He/^{4}He$ reported uncorrected for atmospheric component due to air contamination

3.1. Bulk gas concentrations, $\delta^{13}(CO_2)$ and water measurements

The concentration of CO_2 in the Buttress field is 77 % with the remainder of gas predominately constituting of CH_4 (19.7 %), N_2 (1.9 %) and traces of higher hydrocarbons (0.8 % C_2H_6, 1.1 % C_3H_{10}). Bulk gas compositions for the other two well gases are taken from the literature. CO_2 concentration in the adjacent Boggy Creek field is slightly higher (87%) (Akbari, 1992). The Caroline field has the highest CO_2 concentrations of 99 % with traces of CH_4, N_2 and C_2H_6 (Chivas et al., 1987). All mineral spring gas samples were measured to be above 99 % CO_2 with the remainder of gas composed of noble gases. Glenluce is the only spring showing trace amounts of CH_4 (0.1 %). The $\delta^{13}(CO_2)$ values of the gas samples range from -9.4 to -6 ‰ in springs, and -7.6 to -4.1 ‰ in the well gases. The temperature of the water samples varies from 15.1 – 20.9 °C, pH ranges from 5.6 to 6.3 in CVH springs and 5.5 in Clifton Springs. Total dissolved solids (TDS) values range from 0.63 to 2.85 g/L.

3.2. Noble gas results

$^3He/^4He$ ratios are reported normalised to the value of air (where 1 R_A is the atmospheric ratio of 1.4×10^{-6}). $^3He/^4He$ R_c/R_A are corrected for ^4He derived from the atmospheric component, using the $^4He/^{20}Ne$ value of the sample following the methodology in Craig (1978). It is assumed that all ^{20}Ne is derived from ASW and the $^4He/^{20}Ne$ value of ASW at 20 °C is 0.27 (Kipfer et al., 2002). $^4He/^{20}Ne$ ratios of the well gases are 4-5 orders of magnitude above the ASW value (3097-44656) and range between 0.35 and 326 in the spring samples. $^3He/^4He$ R_c/R_A values differ significantly from the measured $^3He/^4He$ ratios in spring samples with $^4He/^{20}Ne$ ratios <10 (Woolnoughs and Tipperary). Kyneton is the only sample with significant atmospheric contamination ($^4He/^{20}Ne$ = 0.35) which would make the correction erroneous (Sano et al., 2006) therefore its $^3He/^4He$ value is reported uncorrected (1.24 R_A). The $^3He/^4He$ ratios of the remaining spring samples range from 1.23 to 3.65 Rc/R_A. $^3He/^4He$ ratios of well gases from the Port Campbell region are 1.21 and 1.25 R_A. The sample collected from the Caroline CO_2 field in South Australia exhibits a higher value of 3.07 R_A, in agreement with previous measurements (Chivas et al., 1987). All samples are compatible with two-component mixing in a $^3He/^4He$ vs $^4He/^{20}Ne$ plot, where variable $^3He/^4He$ end-members mix with ASW (Fig. 2).

$CO_2/^3He$ ratios of the well gases are within or below the Mid-Ocean Ridge Basalt (MORB) range of 1×10^9 to 1×10^{10} (Marty and Jambon, 1987). This is quite distinct from the higher $CO_2/^3He$ values predicted for near ^3He-free carbonates (O'Nions and Oxburgh, 1988; Sherwood Lollar et al., 1997). CO_2 concentrations in the spring samples are uniform, whilst $CO_2/^3He$ ratios vary over two orders of magnitude, 2.26×10^9 and 6.5×10^{11}, across the typical mantle and crustal values (Fig. 3).

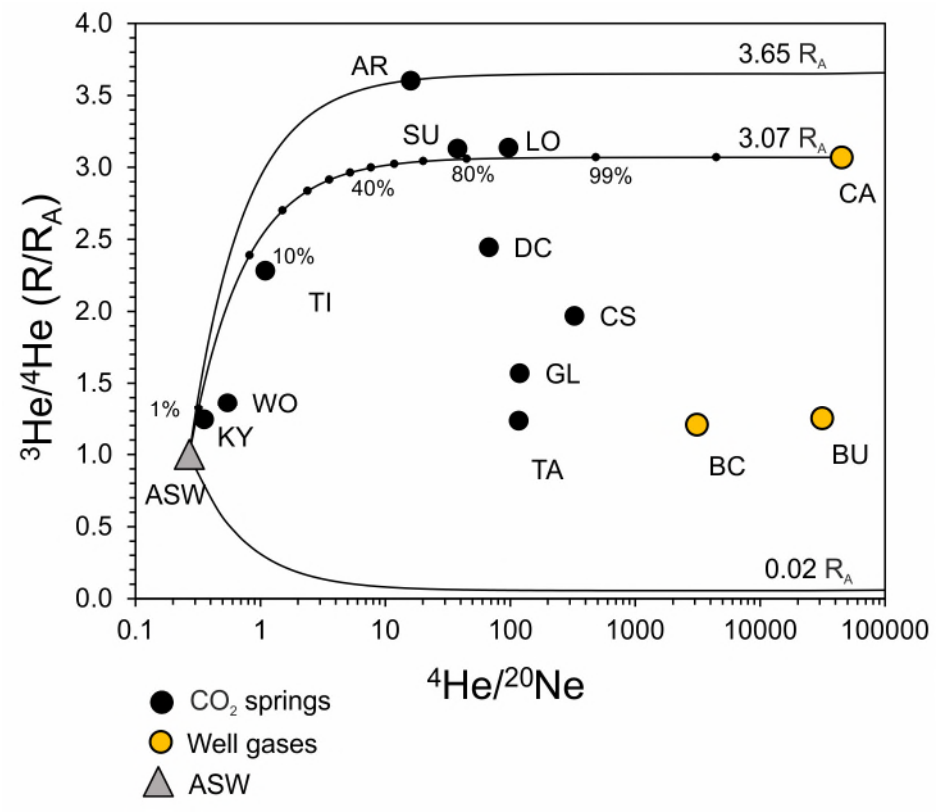

248

249 **Figure 2. ^{3}He/^{4}He R$_A$ plotted against ^{4}He/^{20}Ne ratios of springs and well gases. Solid lines depict binary**
250 **mixing between ASW and the highest regional end-member (Argyle, 3.65 R$_A$), Caroline field and a crustal**
251 **end-member (0.02 R/R$_A$). Black tick marks show percentage of helium from Caroline end-member in the**
252 **mixture. Few springs fall close to the mixing line with the Caroline field, the remaining samples have**
253 **variable amounts of crustal component. The errors are smaller than the symbols. Abbreviations of sample**
254 **names are given in Table 1.**

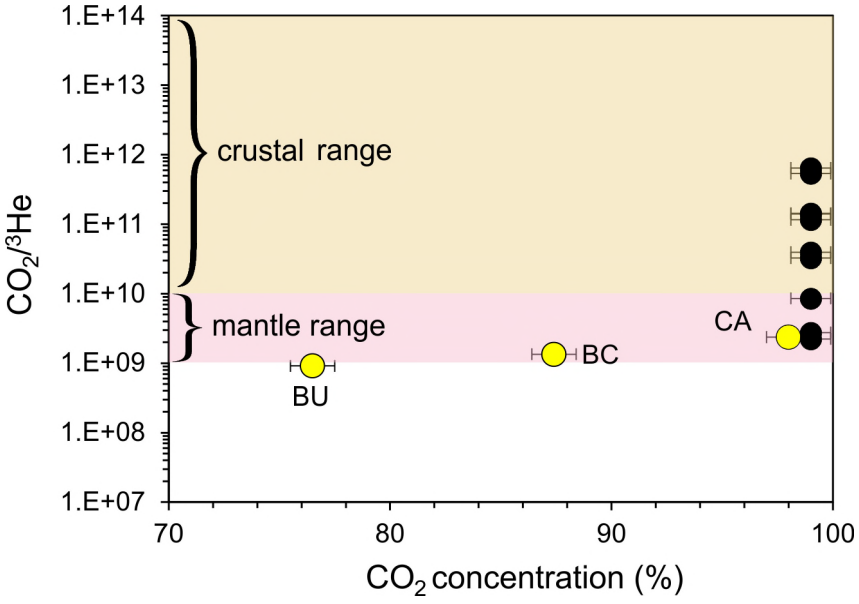

255

Figure 3. $CO_2/^3He$ ratios plotted against CO_2 concentrations for the well gases (yellow circles) and CO_2 springs (black circles). The shaded area shows the range of $CO_2/^3He$ values in the mantle (Marty and Jambon, 1987) and crustal (O'Nions and Oxburgh, 1988) sourced volatiles. Well gas samples are within the mantle range but with positive correlation between $CO_2/^3He$ ratios and CO_2 concentrations. CO_2 concentrations are uniform in the spring samples, however $CO_2/^3He$ ratios are wide-ranging across the typical mantle and crustal values. Vertical errors are smaller than symbols. Abbreviations of sample names are given in Table 1.

Neon, argon, krypton and xenon concentrations were measured in six CO_2 spring samples (Taradale, Locarno, Deep Creek, Glenluce, Woolnoughs and Clifton Springs) (Table 2). $^{20}Ne/^{22}Ne$ ratios of the spring samples range between 9.68 ± 0.05 and 9.92 ± 0.05, close the air value of 9.8 (Eberhardt et al., 1965). $^{40}Ar/^{36}Ar$ ratios range from 299 ± 1 to 323 ± 1, slightly above the value of air (298.5) (Lee et al., 2006). In contrast to relatively uniform and air-like isotope ratios, noble gas concentrations are highly variable. ^{20}Ne concentrations vary over three orders of magnitude (3.43 ± 0.15 x 10^{-8} to 1.4 ± 0.1 x 10^{-5}); ^{40}Ar concentrations vary from 5.3 ± 0.2 x 10^{-5} to 9.44 ± 0.43 x 10^{-4}. ^{84}Kr and ^{132}Xe concentrations range from 8.2 ± 0.3 x 10^{-9} to 7.9 ± 3 x 10^{-8} and 6.5 ± 0.3 x 10^{-10} to 3.6 ± 0.2 x 10^{-9}, respectively.

4. Discussion – link between the CO_2 source in the reservoirs and springs

4.1. He-CO_2 abundance system

The trends in He-CO_2 abundance of well gases and CO_2 springs can be distinguished using a ternary diagram after Giggenbach et al. (1993). This allows depiction of the relative ratios between CO_2-^3He-^4He rather than absolute concentrations (Fig. 4). The MORB end-member (Marty and Jambon, 1987) is displayed for reference with a straight mixing line showing addition of radiogenic ^4He. Caroline, Buttress, and Boggy Creek well gases as well as Argyle and Glenluce springs fall on a mixing line between MORB and crustal end-members. The rest of the springs lie on the mixing trajectory with low He/high CO_2 end-member (the CO_2 apex of the plot).

Based on the observed trends, two main processes can be identified. Addition of radiogenic ^4He to the MORB-type component lowers the $^3He/^4He$, decreases $CO_2/^4He$ and does not affect $CO_2/^3He$ ratio (the trend towards the ^4He apex of the graph). All CO_2 well gas and spring samples exhibit variation in $^3He/^4He$ ratios due to radiogenic ^4He addition. Subsequently, either helium loss or CO_2 addition increases both $CO_2/^3He$ and $CO_2/^4He$ but does not affect the $^3He/^4He$ ratios. The second

process affects the majority of the springs (excluding Glenluce and Argyle) but none of the well gas samples (trajectory towards the CO_2 apex of the plot).

To evaluate this two-step process in the following discussion, we select two samples to use as initial end-members. Argyle spring is representative of the regional high-mantle end member, least affected by radiogenic ^4He addition (exhibiting the highest measured $^3He/^4He$ ratio 3.65 of R_c/R_A, $[^4He] = 8.8 \pm 0.3 \times 10^{-5}$ $cm^3(STP)/cm^3$). The highest He concentrations were measured in Glenluce sample ($^3He/^4He$ 1.57 R_c/R_A, $[^4He]=1.6 \pm 0.1 \times 10^{-4}$ $cm^3(STP)/cm^3$), which is the least affected by secondary He loss or CO_2 addition.

The $^3He/^4He$ ratio can be modified by dilution with non-CO_2 gas (usually methane) with a different He isotopic signature (Sherwood Lollar et al., 1994), radiogenic ^4He accumulation in situ (Newell et al., 2015; Liu et al., 2016) or He stripping from formation water during gas migration through lithological units enriched in ^4He (Sano et al., 1990; Sakamoto et al., 1992). The resulting $^3He/^4He$ ratio can then be overprinted by addition of CO_2 from a different source (O'Nions and Oxburgh, 1988) or phase fractionation during degassing (Matthews et al., 1987). If the well gases and CO_2 springs share a common source, then these processes can be accounted for and gas composition can be traced back to a single initial end-member.

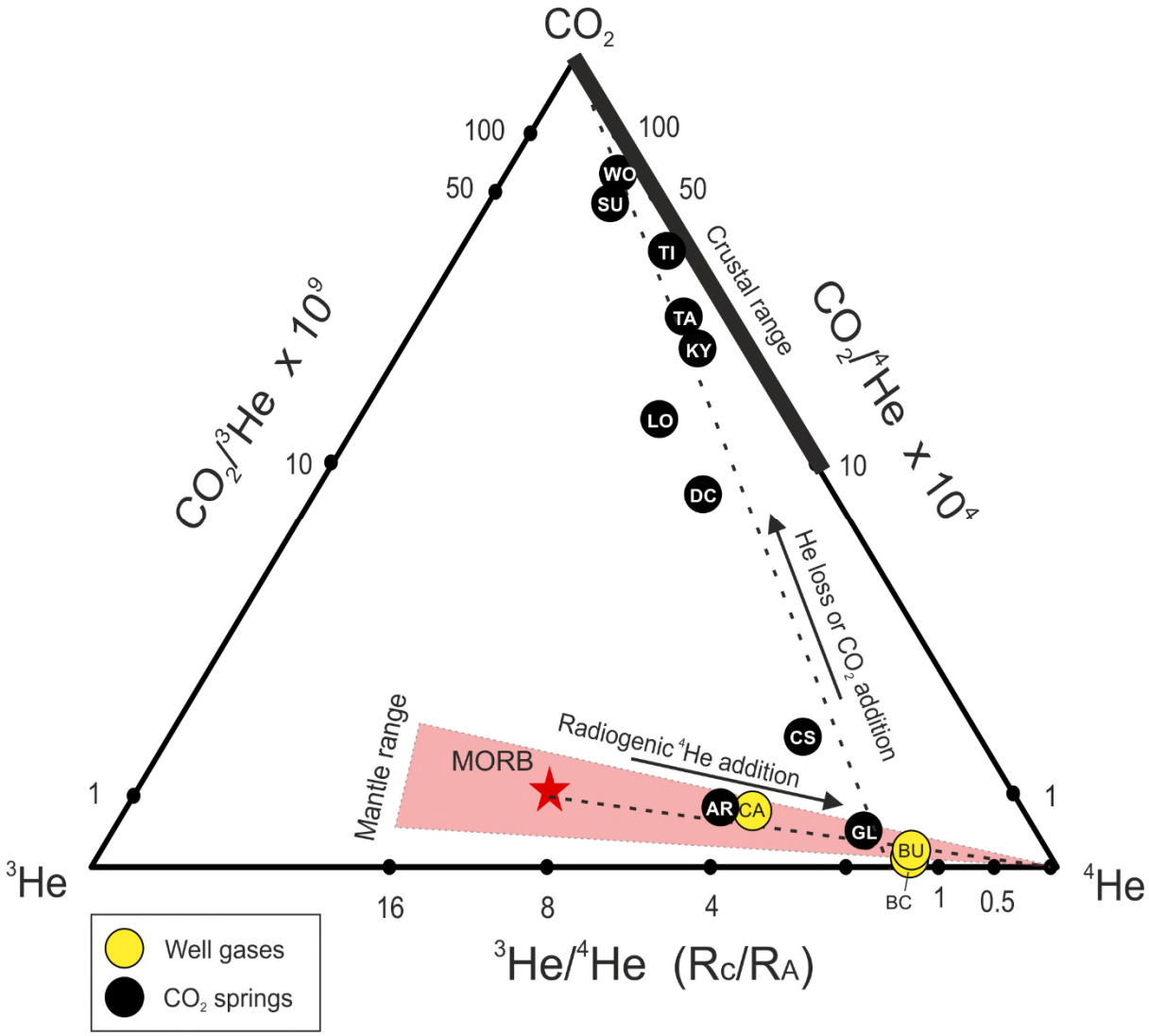

Figure 4. Ternary diagram (after Giggenbach et al., 1993) showing the relationship between the concentrations of CO_2, ^3He, ^4He expressed as their ratios. MORB value used for reference is 8 ±1 R_A (Marty and Jambon, 1987). The dashed lines show mixing between different components. The two clear trends are: 1) Radiogenic ^4He addition, which shifts gas composition to the right apex of the ternary plot, 2) CO_2 addition or He loss trend towards the top apex of the plot. Port Campbell well gases fall on the mixing line between MORB and crustal end-member. Spring samples fall on He loss/CO_2 addition trendline. Abbreviations of sample names are given in Table 1.

4.2 Radiogenic ^4He addition

^4He is produced by the alpha decay of uranium and thorium in the crust. These elements are primarily concentrated in accessory minerals such as zircon and apatite, which release helium at a constant rate above the blocking temperature of the mineral (Tolstikhin et al., 2017). Similarly, ^3He is produced by thermal neutron capture by ^6Li, which can be approximated based on Li content of the crust (Ballentine and Burnard, 2002). However, this contribution is minimal relative to the amount of

^{3}He released from mantle fluids and can be considered to be negligible in the context of in-situ crustal helium accumulation.

After production, radiogenic helium is either trapped in the pore spaces in-situ or mobilised by any migrating water or gas phase present in the subsurface and then transported elsewhere. If a natural gas trap exists in-situ, helium will preferentially accumulate in the gas phase due to its low solubility in water.

4.2.1. Radiogenic ^{4}He accumulation in-situ

The initial ^{3}He/^{4}He ratio of mantle-sourced gas can be reduced by direct accumulation of ^{4}He produced in the crust, or by mixing with ^{4}He-rich methane. The former would be applicable to CO_2 springs, the latter to well gases containing CO_2 and CH_4 mixtures. In both cases, the final ^{4}He concentrations are controlled by the rate of ^{4}He production in the crust. The contents of radiogenic ^{4}He accumulated in-situ in a natural gas trap can therefore be considered as a function of time since the initial emplacement of the gas in the trap, given a known crustal helium production rate (Liu et al., 2016). Under this assumption, we can estimate the residence time required for the observed ^{3}He/^{4}He ratios in both the well gases and the springs.

The ^{4}He production rate (Craig and Lupton, 1976) and ^{4}He concentration in the pore fluid increases at the rate of J_{He} (Torgersen, 1980):

$$^4P = 0.2355 \times 10^{-12} \times [\mathrm{U}] \times (1 + 0.123 \times [\mathrm{Th}]/[\mathrm{U}] - 4) \quad (1)$$

$$J_{He} = {}^4P \times \rho \times (1 - \phi)/\phi)) \quad (2)$$

Where:

$[\mathrm{U}]$, $[\mathrm{Th}]$ – concentrations in ppm

^4P – crustal ^{4}He production rate in cm^3 STP/g yr

J_{He} – ^{4}He production rate cm^3 STP/yr

ρ – density of the crust in g/cm^3

ϕ – porosity of the rocks as a fraction

Assuming ^{4}He has been accumulating in mantle-sourced CO_2 with a known initial composition, the final ^{3}He/^{4}He ratio is expressed as a function of time modified from Newell et al. (2015):

$$^{3}He/\,^{4}He(t) = F \times\ ^{3}He_m/(J_{He} \times\ t\ + \times\ ^{4}He_m) \quad (3)$$

Where:

F – fraction of mantle-sourced gas in the reservoir

He_m – helium concentration of the mantle-source end-member

t – time in years

The final result is independent of the timing of CO_2 emplacement as it records the total ^{4}He accumulated since the start of the gas trap filling, so in the case of CO_2/methane mixture, the recorded age will be that of the methane emplacement. Argyle spring concentrations are taken as representative of the initial mantle-sourced end-member, based on the highest measured $^{3}He/^{4}He$ ratio (3.65 R_C/R_A). This ratio is significantly lower than SCLM or MORB values, but we assume this to be representative of the end-member at the time of emplacement. Similar value is measured in the Caroline field which has likely been emplaced at a similar time to Mount Gambier eruptions dated at 5 ka (Roberston et al., 1996), so we assume this to be a regional feature and that some radiogenic ^{4}He accumulation occurred within the melt before the gas emplacement.

Assuming an average reservoir porosity of 25 % (Watson et al., 2003), average crustal ^{238}U and ^{232}Th concentrations of 2.8 and 10.7 mg/kg and average crustal density of 2.5 g/cm^3 (Rudnick and Fountain, 1995) the estimated age of filling of the of Boggy Creek field is 32 Ma (Fig 5). Assuming ± 5 % and ± 10 % uncertainty in porosity and ^{238}U and ^{232}Th concentrations respectively, the accumulation age could vary between 22 and 45 Ma (showed in shaded area in Fig 5). The model only considers ^{4}He accumulated in-situ and does not account for other ^{4}He sources in the total budget which could include: the initial ^{4}He contents in the gas phase acquired from the source rock, helium stripped from water during the two stages of methane and CO_2 migration in the reservoir and any external ^{4}He flux, caused by heat release associated with regional tectonic events or volcanism. The model also assumes all radiogenic ^{4}He produced in the crust is released into the pore water. Contribution from any of the outlined processes would act to decrease the modelled range, so the calculated accumulation age range can therefore be taken as a maximum estimate.

Methane in Port Campbell traps is associated with the last hydrocarbon generation stage that commenced during the mid-Paleogene (Duddy, 1997; Boreham et al., 2004), which closely matches the range of accumulation ages calculated. The $^{3}He/^{4}He$ ratios observed within the Boggy Creek and Buttress fields can plausibly be explained by an Argyle-type end-member mixing with methane containing radiogenic ^{4}He, confirming the binary mixing with methane trend depicted in Figure 4.

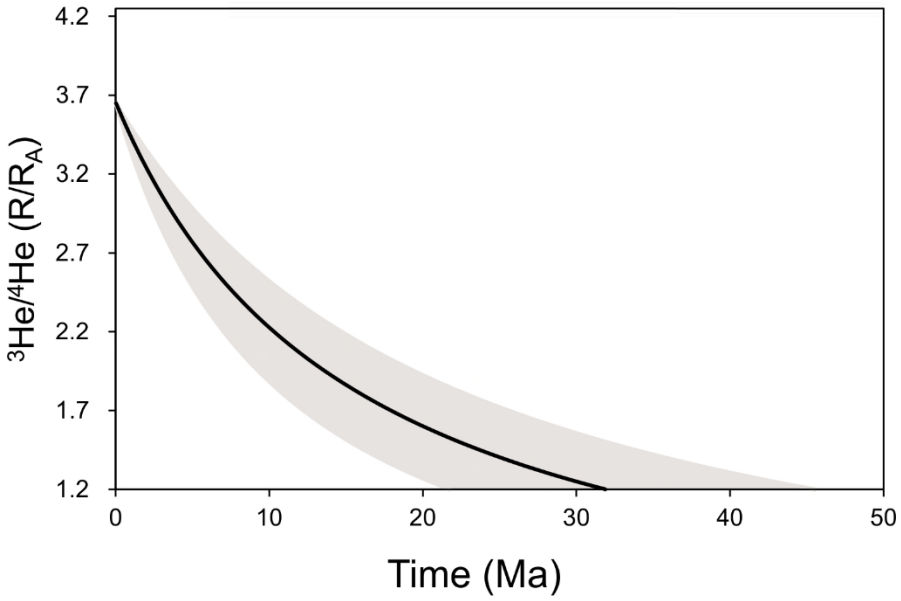

375

376 **Figure 5. $^3He/^4He$ ratio vs time since gas emplacement calculated for the composition of the Boggy Creek-1**
377 **sample. To achieve the current $^3He/^4He$ ratio measured in Boggy Creek (1.21 R_A), Argyle-type CO_2 (3.65 R_A)**
378 **would have to mix with methane that has been emplaced at 32 Ma. Shaded area shows uncertainty.**

379 The same calculation can be applied to the CO_2 springs. The ^{238}U-^{232}Th contents are assumed
380 to be the same; the porosity of a fracture-dominated metasedimentary aquifer is estimated to be
381 lower (10 ± 5 %). To reduce the initial $^3He/^4He$ ratios of 3.65 to the lowest measured value of 1.23 R_A,
382 it would take 9 Ma years on average and between 4-15 Ma within the uncertainty of the parameters.
383 To account for the range of observed $^3He/^4He$ ratios, this scenario requires emplacement of separate
384 gas pockets for each individual spring at different times between 9 Ma and present and retention
385 within the crust before the onset of the recent migration to the surface.

386 Multiple gas injection events could be associated with discrete episodes of seismic or volcanic
387 activity, although the latter is unlikely because the volcanic cones are far fewer than the individual
388 mineral springs (>100) (Shugg, 2009), and given the predominately monogenetic eruptive character
389 of the NVP extrusives (Boyce, 2013) volcanic activity is unlikely to produce so many different gas
390 pulses. Irrespective of the gas emplacement mechanism, the heavily folded and fractured Ordovician
391 metasedimentary sequence is unlikely to act as an effective gas trap for millions of years. In-situ ^4He
392 accumulation in CO_2 springs is therefore an unlikely process to account for the observed variation in
393 $^3He/^4He$ ratios.

394 4.2.2. Radiogenic ^4He stripping from enriched pore-water

395 An alternative model to in-situ generation is modification of magmatic $^3He/^4He$ ratios by
396 dilution of mantle He by interaction with radiogenic helium-rich basement fluids during lateral

movement of the CO_2. Stagnant fluids in basement rocks with high U/Th concentrations are enriched in radiogenic ^4He well above ASW levels with $^3He/^4He$ ratios in the crustal range (0.02 R_A) (Bottomley et al., 1984; Weinlich et al., 1999; Holland et al., 2013; Warr et al., 2018). Isolated stagnant pockets of these fluids within the Cambrian – Ordovician basement sequence are a likely source of ^4He for the migrating mantle CO_2. In this case, the process is still governed by the helium production rate in the crust (similar to the in-situ ^4He accumulation discussed above), but the controlling factor is distance migrated through the basement rather than time.

Samples with higher $^3He/^4He$ ratios are located geographically closer to each other and the Muckleford fault zone. Under the assumption that one of these major fault zones could provide a pathway for mantle CO_2 ascent to the surface, we can infer that the spring with the highest measured $^3He/^4He$ ratio (Argyle, 3.65 R_A) would be the closest to the main conduit. Figure 6a shows the relationship between the $^3He/^4He$ ratios and the radial distance of sample location to the Argyle spring. Kyneton spring is excluded from this because of its contamination with an atmospheric component. The observed $^3He/^4He$ ratios consistently decrease with increasing distance from the inferred conduit, suggesting mantle CO_2 is being progressively diluted with a crustal component with increasing distance migrated through the basement.

The mechanism of interaction with these fluids depends on whether CO_2 migrates in the gas phase or dissolved in water. In case of the former, the governing factor is differences in solubility as helium is strongly partitioned from the fluid to the migrating gas phase. If CO_2 migrates dissolved in water, the mixing with the crustal fluids can be described by a mechanical dispersion model (Sano et al., 1990). Assuming that mantle fluids are supplied through a single conduit at a constant rate under steady-state homogeneous and isotropic conditions under an equal hydrostatic pressure, $^3He/^4He$ is calculated as a function of the radial distance to the conduit (r) following the approach detailed in Sano et al. (1990) of deriving the location-specific helium dispersion constant (α) by fitting a least squares function to the measured $^3He/^4He$ and radial distance data points.

$$^3He/^4He(r) = (\,^3Pr^2 + \alpha\,^3He_m)\,)/(\,^4Pr^2 + \alpha\,^4He_m)) \quad (4)$$

Where:

r – radial distance from the main gas conduit

α – helium dispersion constant, dependent on the pore network geometry

P – crustal helium production rate in atoms/cm^{3}s, calculated under the same crustal density and U, Th content assumptions as in the ^4He accumulation model.

Similar decreases in $^3He/^4He$ ratios with increasing distance from a central volcanic cone has been observed in various active volcanoes (Marty and Jambon, 1987; Williams et al., 1987; Sano et al., 1990; Sakamoto et al., 1992). The calculated hydrodynamic dispersion coefficient (methods in Sano et al., 1990) is 0.035 cm^2/s, which compares well with the estimates in the original model (0.09 and 0.055 cm^2/s).

The overall average rate of $^3He/^4He$ decrease in 4 volcanic locations reviewed by Sakamoto et al. (1992) varied between 0.3 to 0.5 R_A/km. The average rate of $^3He/^4He$ decrease in CVH is 0.1 R_A/km, potentially reflecting fluid migration via more efficient fracture networks and conduits in a faulted sequence relative to the previously investigated volcanic and volcanoclastic sequences. Fractured aquifers have lower tortuosity relative to porous ones, which results in shorter effective travel distance for the same total flow path distance (Clennell, 1997) and therefore lower rate of interaction with radiogenic basement fluids per distance travelled.

Springs with the highest $^3He/^4He$ ratios are clustered near the N-S trending Muckleford Fault and a smaller parallel fault striking along Lake Daylesford (Fig 6b). Previous studies have shown that clusters of NVP volcanic vents are commonly aligned parallel to nearby basement faults throughout the province (van Otterloo et al., 2013; Cas et al., 2017). Mantle xenoliths were found in the vicinity of the faults, suggesting fast mantle upwelling rates through the lithosphere were prevalent during periods of magmatic activity (van Otterloo et al., 2014). While further work is required to provide geomechanical and structural geological evidence for current fluid migration along the fault zones in the CVH, the spatial distribution of $^3He/^4He$ ratios suggests that these basement lineaments potentially play an important role in the currently active mantle-CO_2 ascent to the surface.

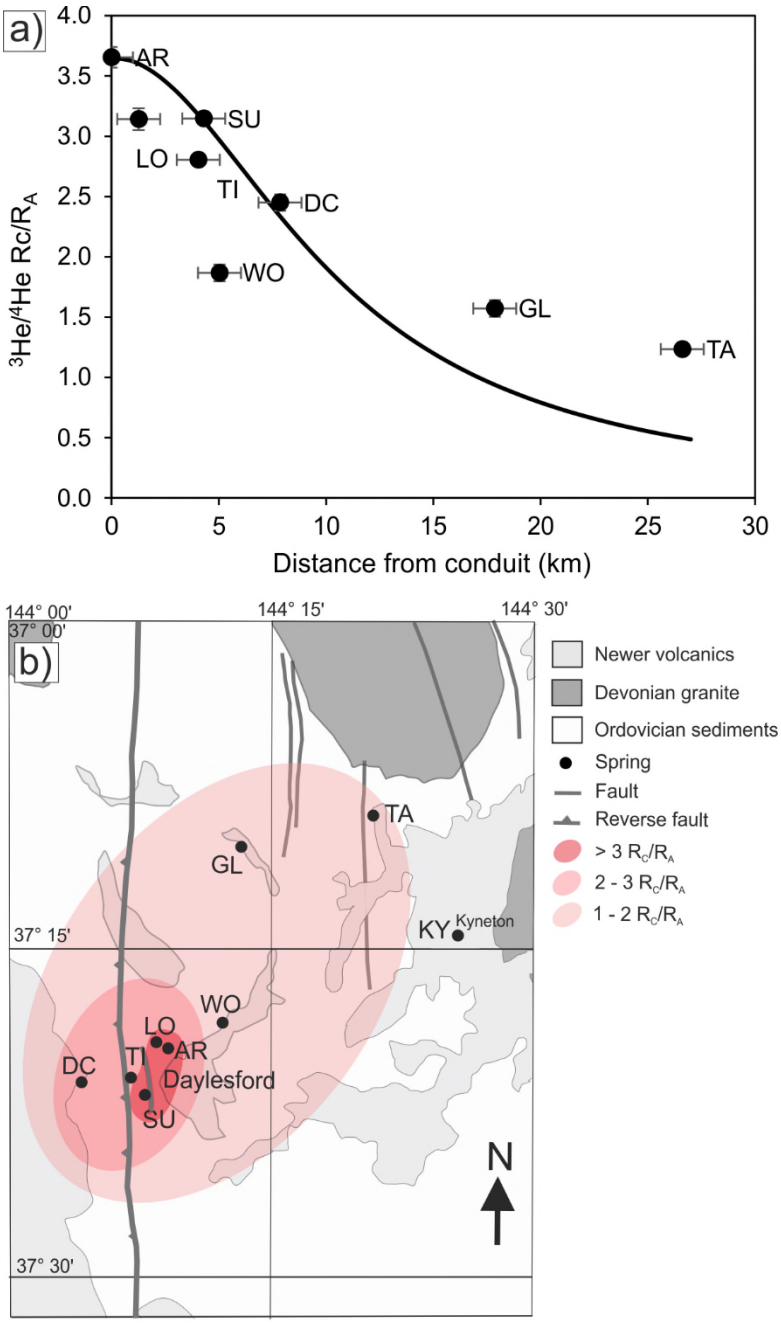

449

450 **Figure 6 a). Plot of ^{3}He/^{4}He R_c/R_A values relative to the distance from the Argyle spring (highest ^{3}He/^{4}He**
451 **ratio), inferred to be closest to the conduit. ^{3}He/^{4}He ratios decrease with increasing radial distance. The**
452 **solid line is ^{3}He/^{4}He dispersion with distance model calculated based on Sano et al. (1990). b) Geographical**
453 **distribution of CO_2 springs. Springs with the highest ^{3}He/^{4}He ratios are clustered close to N-S trending**
454 **basement-scale Muckelford thrust fault and parallel smaller fault near Lake Daylesford. Shaded areas show**
455 **^{3}He/^{4}He ratio ranges which decrease with increasing distance from the Argyle spring. Kyneton spring is**
456 **excluded due to atmospheric contamination. Abbreviations of sample names are given in Table 1.**

4.3. Evaluating models to account for $CO_2/^3He$ and $\delta^{13}C(CO_2)$ variation

The combination of CO_2, helium and $\delta^{13}C(CO_2)$ values is commonly used to identify the presence of mantle volatiles. This is because $CO_2/^3He$ ratios have been well constrained for mantle-derived melts, fluids and volatiles, with an average MORB value accepted as $1.5 \pm 0.5 \times 10^9$ (Sano and Marty, 1995; Marty and Tolstikhin, 1998). ^3He is not produced in significant amounts in the crust, so low $^3He/^4He$ ratios and associated $CO_2/^3He$ ratios between $10^{10} – 10^{15}$ are typically associated with a crustal CO_2 source (O'Nions and Oxburgh, 1988). The $CO_2/^3He$ ratios observed in ten CO_2 samples from the Victorian mineral springs vary over two orders of magnitude (2.8×10^9 to 6.5×10^{11}), encompassing the range typical of mantle and crust end-members. A trend in increasing $CO_2/^3He$ ratios is therefore commonly associated with admixture of crustal CO_2 and/or degassing in open system (e.g. Crossey et al., 2009; Newell et al., 2015; Ruzié et al., 2013), defined by Rayleigh fractionation. Here, we test both of these possibilities.

Crustal end-members can have a wide range of $CO_2/^3He$ ratios but a narrow range of $^3He/^4He$ ratios (0.01 – 0.07 R_A) (Ozima and Podosek, 2002). Figure 7 shows $CO_2/^3He$ values plotted against $^3He/^4He$ R_c/R_A ratios with binary mixing curves representing mantle (8 R_A) source and various crustal components. Significantly, samples with high $CO_2/^3He$ ratios do not necessarily show lower $^3He/^4He$ ratios, as would be expected in the case of mixing with ^3He-poor crustal CO_2 source and trend perpendicular to the calculated mixing lines. To explain the range of measured $CO_2/^3He$ ratios, variable amounts of mixing with a wide range of different crustal reservoirs ($CO_2/^3He$ – 10^{10} - 10^{14}) would need to be invoked, which is unlikely in the setting where bedrock lithology is uniform across the area.

Crustal CO_2 addition can be further assessed by combining He data with $\delta^{13}C(CO_2)$ values (Sano and Marty, 1995). The range of $\delta^{13}C(CO_2)$ values measured in the springs (-9.4 to -6‰) partly overlap the typical mantle range (-7 to -4‰) (Wycherley et al., 1999). However, increasing $CO_2/^3He$ ratios do not consistently correlate with $\delta^{13}C(CO_2)$ change towards carbonate or organic end-members (Fig. 8). Instead, a vertical trend exists, which would require mixing with an end-member with constant proportions of both organic and carbonate-sourced CO_2. To explain the highest observed $CO_2/^3He$ ratios, 99 % of non-mantle (crustal/organic mixture) CO_2 addition is required. Such significant amounts of crustal CO_2 sourced by dissolution of bedrock minerals would liberate cations contained in the dissolving minerals and increase the TDS values of the water. Figure 9 shows that there is no clear positive correlation between the $CO_2/^3He$ ratios in the volatiles and TDS values in their associated waters. Alternatively, CO_2 and helium loss during open system degassing can be evaluated using Rayleigh fractionation modelling. Figure 8 also shows a calculated open system

Rayleigh fractionation line, assuming average pH of 6.1 and 15 °C temperature. The calculated fractionation factor between He/CO_2 is 0.012; the enrichment factor $ln10^3\alpha$ $\delta^{13}C(CO_2)_{aq}/(CO_2)_g$ is 2.2‰. Open system degassing under measured conditions would result in a similar fractionation in $CO_2/^3He$ ratio but a significantly more extensive than observed fractionation of $\delta^{13}C(CO_2)$ values. We therefore conclude that degassing under open system conditions is not supported by the data.

Previous geochemical modelling work showed that CO_2 does not cause significant amounts of bedrock mineral dissolution in the Ordovician aquifer (Karolytė et al., 2017) and there is no geological evidence for addition of large amounts of crustal CO_2 from other sources (e.g. carbonate metamorphism). The possibility of significant amounts of organic CO_2 addition is also ruled out, because the observed trend on Figure 8 cannot be explained by addition of organic CO_2 in the absence of the crustal component. Based on the combined evidence from $\delta^{13}C(CO_2)$-He, CO_2 abundance and TDS contents of the mineral waters, we conclude that there is no significant crustal CO_2 addition to the mantle volatiles sampled at the CVH and Clifton Springs. CO_2 loss during degassing under open system conditions is also not supported by the data.

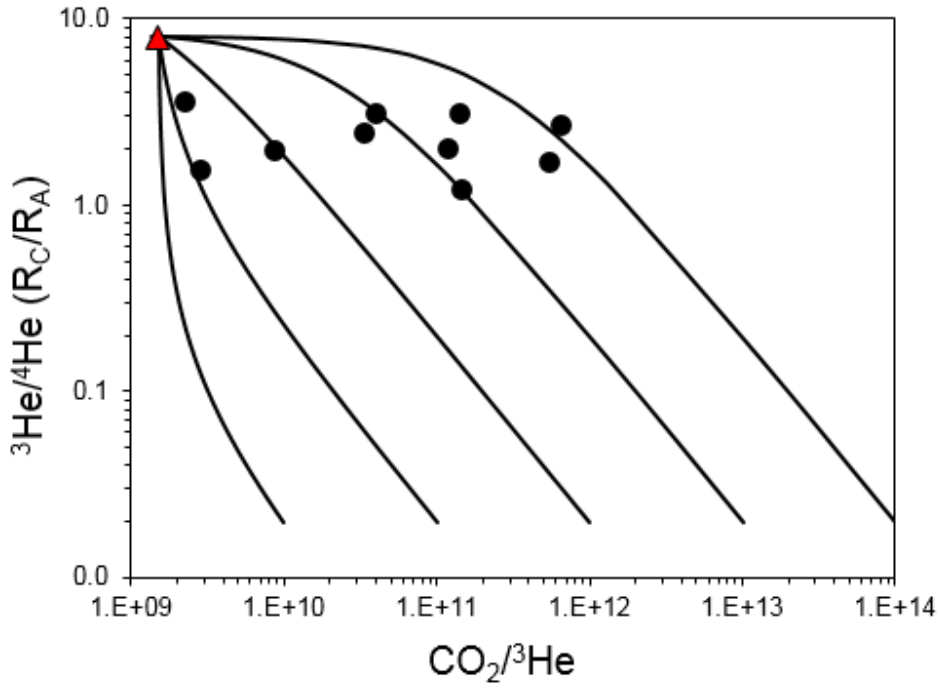

Figure 7. Binary mixing plot between MORB (red triangle) ($^3He/^4He$ 8 R_A, $CO_2/^3He$ 1.5 x 10^9) and various crustal end-members ($CO_2/^3He$ 10^{10}-10^{14}). The springs form a near-horizontal trendline and do not follow any of the mixing lines, suggesting that mixing does not control the variation in $CO_2/^3He$ values. All error bars are smaller than the printed symbols.

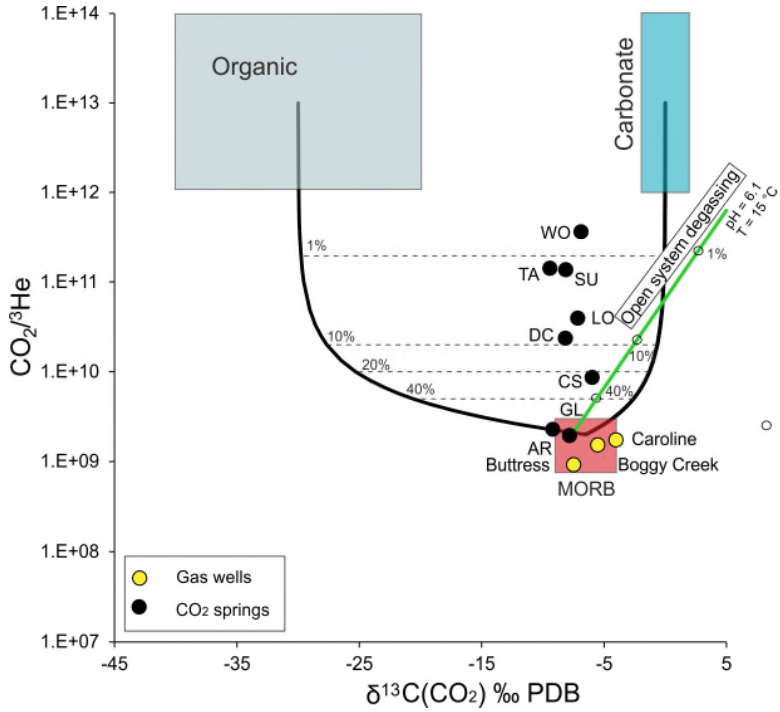

509

510 **Figure 8. $CO_2/^3He$ ratios vs $\delta^{13}C(CO_2)$ values for gas samples in relation to mixing between the mantle,**
511 **carbonate and organic CO_2 end-members based on Sano and Marty (1995). Caroline, Boggy Creek and**
512 **Buttress well gases fall within the mantle range. Spring samples do not show a coherent trend towards**
513 **either an organic or carbonate CO_2 end member. The observed trend would require > 99% contribution of a**
514 **component with constant proportions of both organic and carbonate-sourced CO_2. Green line shows**
515 **Rayleigh fractionation during degassing under average measured pH and temperature, open circles indicate**
516 **percentage of gas left. The data do not fall on either the mixing or open system degassing curves (discussed**
517 **in text). Abbreviations of sample names are given in Table 1.**

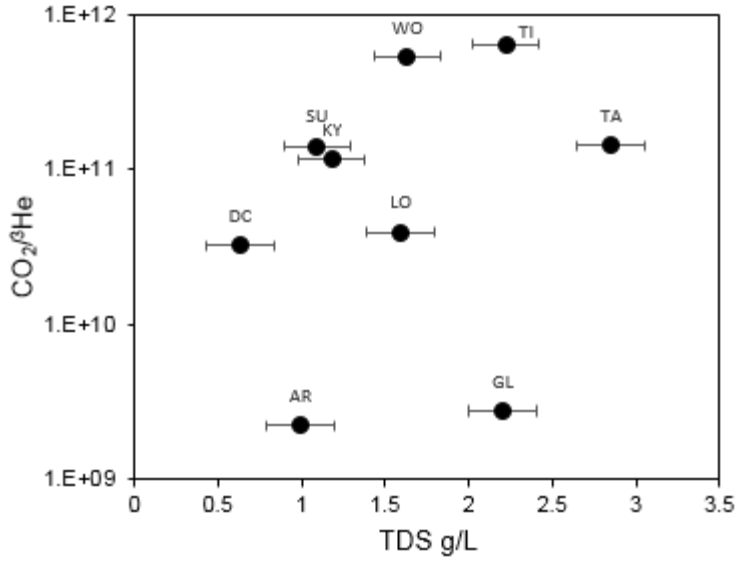

Figure 9. $CO_2/^3He$ vs TDS measured in water, sampled via hand pumps from tube bores. $CO_2/^3He$ values are not correlated with TDS. A positive correlation would be expected if crustal CO_2 were added as a result of bedrock mineral dissolution.

Alternatively to mixing with different CO_2 sources, the variability of $\delta^{13}C(CO_2)$ values (-9.4 to -6‰) can be explained by degassing in separate individual systems under a range of different pH and temperature conditions. Equilibrium fractionation between $\delta^{13}C(CO_2)$ in aqueous and gaseous phases is controlled by the temperature and the relative amounts of HCO_3^- and H_2CO_3, which are pH-dependent. If H_2CO_3 is the dominant dissolved inorganic carbon (DIC) species, degassing CO_2 is slightly enriched in ^{13}C. Conversely, when HCO_3^- dominates the system, degassing CO_2 is relatively depleted in ^{13}C (Deines et al., 1974). The pH values measured in mineral water bores range from 5.5 to 6.1 and temperatures are 15 – 21 °C. In this particular range of conditions, the ratio of HCO_3^- to H_2CO_3 in DIC varies significantly. The resulting calculated equilibrium enrichment factors between DIC and gaseous CO_2 range from -3.4 to -0.43‰. Degassing under different DIC speciation conditions therefore can fully account for the observed 3.4‰ variability in $\delta^{13}C(CO_2)$ values of the spring gases.

The trends observed in our data are not unique to this study. $CO_2/^3He$ ratios ranging between 10^9 to 10^{14} combined with $\delta^{13}C(CO_2)$ values without an obvious trend towards organic of carbonate end-member is a common observation, commonly interpreted as a result of simple mantle and crustal end-member mixing (Aka et al., 2001; Crossey et al., 2009; Mao et al., 2009). Other workers recognised that simple mixing is not a conclusive interpretation (Italiano et al., 2014) and suggested contribution of a solubility fractionation process (Matthews et al., 1987; Hilton, 2009; Newell et al., 2015). Where open system Rayleigh fractionation is proposed, it is commonly not conclusively supported by evidence from $\delta^{13}C(CO_2)$ values (Ruzié et al., 2013; Bräuer et al., 2016). In the following

section, we explore how this trend can alternatively be explained by fractionation during a two-step process of dissolution and degassing.

4.4 Noble gas abundance modification by solubility in water

The variation observed in ^{3}He concentrations in the mineral spring samples is also replicated in ^{4}He and other noble gases. Figure 10 shows the distribution of noble gas concentrations in all studied springs. Importantly, the variance in observed gas concentrations decreases with element mass (Fig. 10), indicating a solubility-controlled process. If mantle CO_2 is transported to the surface in solution, this process can be modelled as dissolution and subsequent degassing.

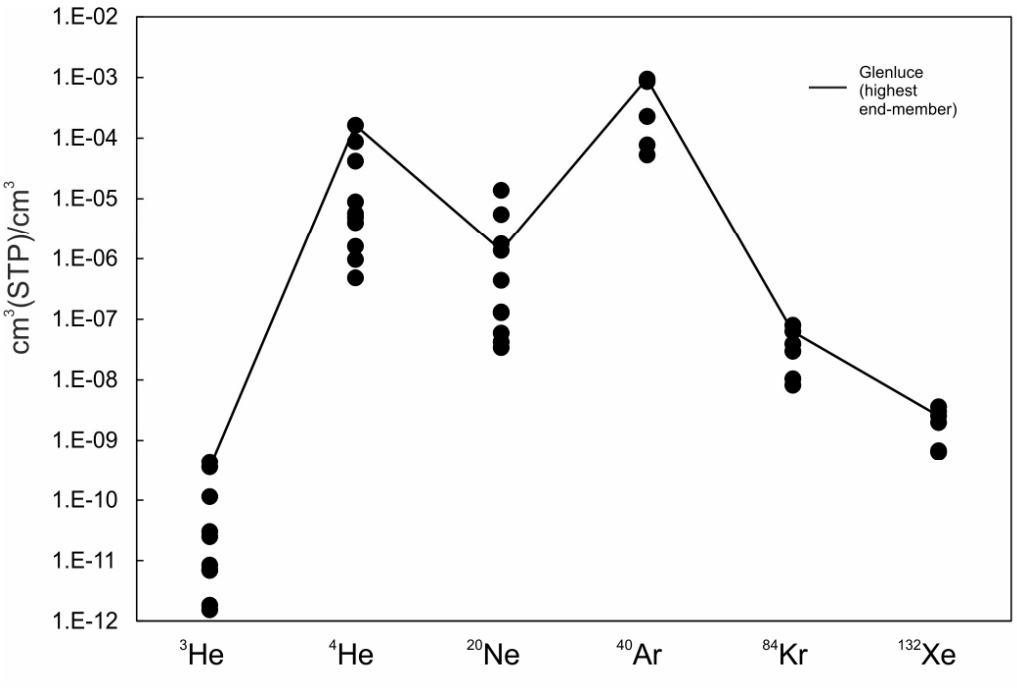

Figure 10. Noble gas concentrations of CO_2 spring samples in cm^3 (STP)/cm^3. The variation in concentrations decreases with increasing molecular mass. Solid black line shows the concentrations measured in Glenluce spring, which has the highest helium concentrations and least fractionated $CO_2/^3He$ ratios.

During the equilibration between gas and water, noble gases are partitioned between the phases according to their solubility coefficient, as defined by Henry's Law:

$$C_{iw} = \frac{C_{ig}}{K_i} \quad (5)$$

Where C is concentration, subscripts g and w denote gas and water phases and Ki is dimensionless Henry's constant for noble gas i. Ki is temperature, pressure and salinity dependent (Kipfer et al., 2002). The final concentrations in both phases depend on the volumetric gas/water ratio. The equilibrium concentrations in the water (C_{iw}^{eq}) are expressed as (Zartman et al., 1961):

$$C_{iw}^{eq} = C_{it} \times F_w \quad (6)$$

$$F_w = \frac{C_{iw}V_w}{C_{iw}V_w + C_{ig}V_g} \quad (7)$$

Where V is volume, C_{it} is the total noble gas budget, and F_w is the fraction of noble gases in the water. Combining equations 5-7, C_{iw}^{eq} is:

$$C_{iw}^{eq} = C_t \times (1 + \frac{V_g}{V_w} K_i)^{-1} \quad (8)$$

After the equilibration step, the water and the gas source separate and ascend to the surface independently. The gases collected at the surface of stream beds are assumed to have been transported in solution. During degassing at the surface, the noble gases are partitioned between the phases again. The final measured gas concentrations are:

$$C_{ig}^{f} = C_{iw}^{eq} \times (1 + (\frac{V_g}{V_w})^{-1} \frac{1}{K_i})^{-1} \quad (9)$$

For the purpose of investigating a shallow degassing process, equilibration with fresh water at atmospheric pressure and 20 °C temperature is assumed. Henry's constants and activity coefficients for water conditions were calculated from empirical equations from Crovetto et al. (1982) for Ne, Ar, Kr and Xe and Smith (1985) for He, following the methodology in Ballentine and Burnard (2002). Henry's constant for CO_2 is calculated using empirical equations from Crovetto (1991). Assuming the density of fresh water (0.996 cm^3/g) (Weast et al., 1988), concentrations in ASW are converted from cm^3STP/g_{H2O} to cm^3STP/cm^3 for Figure 11.

The highest helium concentrations and lowest $CO_2/^3He$ ratio were measured in the Glenluce spring. We therefore assume that Glenluce is the least solubility fractionated end-member. For the purpose of the model, we make a simplifying assumption that the Glenluce sample represents the total amount of CO_2 and noble gases from both the mantle and ASW sources (C_t). This end-member equilibrates with a volume of water which, in theory, is noble gas free. When $\frac{V_g}{V_w} \to 0$, $F_w \to 1$, all gases are dissolved in water. All gas contents are transferred into the water phase C_{iw}^{eq} and the ratios are equal to the initial ones. When $\frac{V_g}{V_w} \to \infty$ and $F_w \to 0$, only a small fraction of noble gas contents are dissolved in water. In this case, the ratios are the most fractionated and the concentrations in water are low. After the equilibration, the water separates from the gas source, migrates to the surface and degasses. We make a simplifying assumption that the water degasses entirely, $\frac{V_g}{V_w} \to \infty$, all dissolved gases are transferred into the gas phase and therefore the final measured $C_{ig}^{f} \to C_{iw}^{eq}$.

589 Figure 11 shows CO_2/He ratios, ^{3}He concentrations relative to ^{4}He, ^{20}Ne, ^{40}Ar, ^{84}Kr and ^{132}Xe and the
590 calculated solubility curves C_{ig}^{f}. The data points fall on the modelled line and is clearly
591 distinguishable from mixing with ASW, which is more enriched in all atmospheric noble gases. Air
592 and ASW components are potentially introduced by inclusion of small amounts of air and water into
593 the copper tube during sampling and are the most significant in Kyneton, Tipperary and Woolnoughs
594 samples. Tipperary and Woolnoughs springs include a combination of ASW and air components,
595 which is obvious in different element pair plots (Fig. 11 c,d,e,f) and less apparent in ^{3}He vs ^{4}He (Fig.
596 11b) because air and ASW have similar ^{3}He/^{4}He ratios. Figure 11b also clearly shows that the original
597 concentrations in Kyneton spring have been overprinted by admixture of air, most likely during
598 sample collection and clearly identified in the ^{4}He/^{20}Ne ratios. The ASW component is more evident
599 in the heavier atmospheric noble gases in the Deep Creek sample (Fig. 11 ,d,e,f).

600 With the exceptions discussed above, all other samples plot close to the modelled solubility
601 fractionation line. The maximum extent of fractionation between CO_2 and He is limited by the ratio
602 of Henry's constants K_{CO2}/K_{He} (Fig. 11a). The calculated $\frac{V_g}{V_w}$ ratios and progressive loss of noble gas
603 concentrations with decreasing F are consistent across all noble gas elemental pairs. When $\frac{V_g}{V_w}$ is
604 unity, 47% of the total CO_2 is dissolved but only 1% of helium. The resulting CO_2/^{3}He ratio is 1.4 x
605 10^{11}, which is the highest in the sample group, excluding the previously discussed samples which are
606 contaminated with air. This means that dissolution in water under equal gas/water ratios explains
607 the maximum observed fractionation of CO_2/^{3}He values. According to the model, the minimum $\frac{V_g}{V_w}$
608 ratio required to dissolve the entire sample without fractionating the CO_2/^{3}He is 0.0005, or 2000
609 times more water than gas.

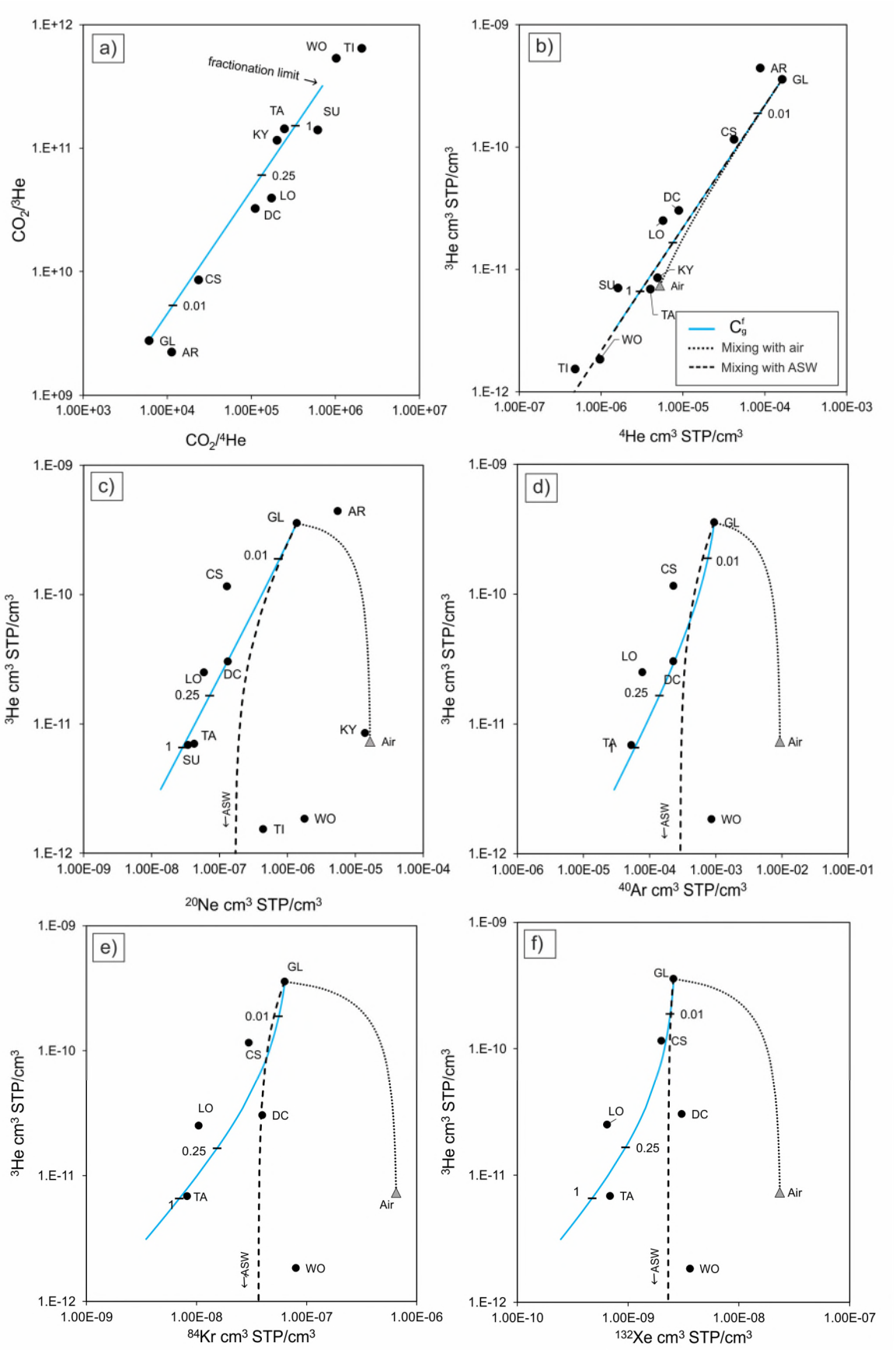

Figure 11. CO_2/He ratios (a) and ^{3}He concentrations relative to ^{4}He (b), ^{20}Ne (c), ^{40}Ar (d), ^{84}Kr (e) and ^{132}Xe (f) in cm^3(STP)/cm^3. The solid blue line shows the concentrations in the gas phase after a two-step dissolution

and degassing. First, water equilibrates with gas under different gas/water ratios. Second, the water of that composition degasses entirely. Tick marks show gas/water ratios during the dissolution stage. Dashed lines show mixing with ASW at 20 °C; dotted line shows mixing with air. Some deviations from the modelled line occur due to mixing with ASW and/or air. a) The extent of CO_2/He fractionation during dissolution is limited by K_{CO2}/K_{He}. All samples fall within this range except for TI and WO. c) shows that this is because TI and WO have a contribution between ASW and air components, plotting between these end-members. This is consistently replicated for Woolnoughs spring in c) d) and e). Ar, Kr and Xe concentrations of CS, DC, LO and TA springs are within the limits of mixing with ASW and calculated model line. Abbreviations of sample names are given in Table 1.

The model results are not a strict interpretation of the geological system, but rather an indication of how the water controls the noble gas budget. The samples with high noble gas concentrations and mantle $CO_2/^3He$ ratios might alternatively be interpreted to represent the residual gas cap migrating the gas phase after the equilibration with water or having had minimal interaction with the water. However, in cases where gas migrates dissolved in water and degasses at the surface, equilibration in equal volumes of gas and water is needed to fractionate the $CO_2/^3He$ ratios by two orders of magnitude. This is a significant consideration for the use of $CO_2/^3He$ ratios in interpretation of gas provenance in gases equilibrating with water.

Figure 12 shows a theoretical fractionation model of mantle-derived CO_2 under the same ambient atmospheric conditions as the previous model. A sample with the starting concentrations of [CO_2] = 0.99 and [^3He] = 1.2 x 10^{-12} cm^3STP/cm^3 is dissolved in water under different gas/water ratios. The figure shows how the decreasing fraction of moles relative to the starting value, transferred to the water and gas phases during the two-stage process, translates to $CO_2/^3He$ ratios. When the gas/water ratio is low during the dissolution step, all gasses are dissolved into the water phase and the ratio is unchanged. As the gas/water ratio decreases, overall less gas is transferred into the water phase, but the water becomes more enriched in CO_2 relative to helium. The second step considers degassing after the equilibration, when the remaining non-dissolved gas is removed from the system and the water degasses under three scenarios ($\frac{V_g}{V_w} \rightarrow 0$, 0.25 and 1). This effectively shows that in a multi-step dissolution and degassing process, the $CO_2/^3He$ ratio is entirely dependent on the gas/water ratios and the extent of fractionation is limited by the ratio of Henry's constants K_{CO2}/K_{He}. In practice, the process is relevant to the point where the gas concentrations are above those in ASW and the signal is not entirely diluted. Where CO_2 is the main carrier gas, this effect may not be intuitively obvious, because the measured CO_2 concentrations are always > 99 % and the observed variation is the ^3He concentrations.

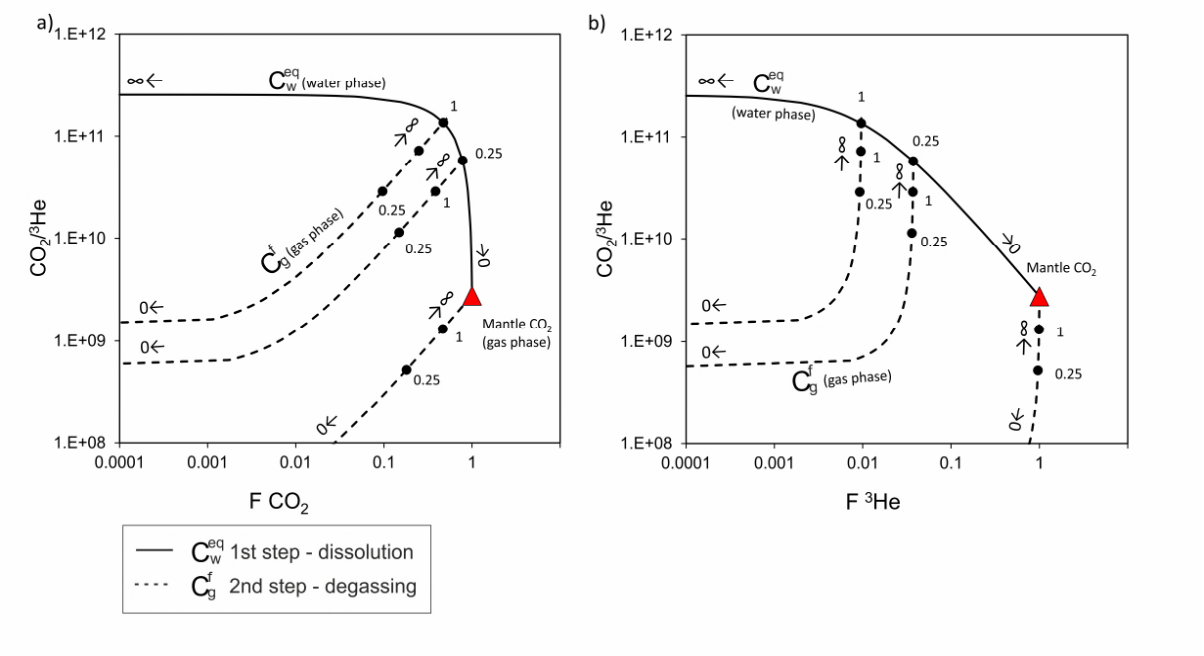

Figure 12. Theoretical model of two step dissolution and degassing of mantle CO_2 and the effect on the $CO_2/^3He$ ratio. F is the fraction of moles in the modelled phase relative to the starting value. Symbols with arrows indicate $\frac{V_g}{V_w}$ ratios approaching infinity and zero, black dots mark specific calculated ratios. The solid black line shows the water phase during dissolution stage (step 1). The dashed lines show the resulting gas phase after degassing of the water phase under three different scenarios ($\frac{V_g}{V_w}$ ->0, 0.25, 1) (step 2). The maximum fractionation of $CO_2/^3He$ is limited by the relative ratio of K_{CO2}/K_{He}.

4.4.1. Summary

The geological interpretation of the proposed solubility fractionation model requires two stages of phase separation - dissolution followed by degassing. Mantle CO_2 equilibrates with individual aquifers under different gas/water ratios. Following this, CO_2-saturated water and the remaining gas separate and ascend independently, driven by the differences in buoyancy force. Continuous seepage of dry CO_2 (up to 6000 ppm) has been identified in the localised fractures of the Ordovician sandstone outcropping near the Tipperary spring (Roberts et al., 2019), confirming the decoupled CO_2 and water migration. Water migrates to the surface through individual conduits, forming individual mineral water bodies and eventually springs. This model is consistent with the $\delta^{13}C(CO_2)$ data, explained by degassing under measured temperature and pH conditions with each spring acting as a separate system. This appears to be a plausible interpretation of the CVH mineral springs, which show high variability in dissolved carbon and cation contents, indicating restricted individual aquifers for separate springs (Cartwright et al., 2002; Weaver et al., 2006). Mineral water degasses at the surface and all noble gases and CO_2 are assumed to be stripped from the water phase. The

final measured noble gas budgets are strongly controlled by the initial stage of equilibrating with water.

4.5 Model summary and application to CO_2 tracing

This case study of south-east Australian CO_2 gas reservoirs and natural springs provides a framework for investigating genetic link between CO_2 stored in reservoirs and migrating into shallow aquifers. Our findings suggest that the combined helium, CO_2 abundance and $\delta^{13}C(CO_2)$ system allows to distinguish between key processes that modify the initial geochemical composition: admixture of crustal or organic sourced CO_2, mixing with non-CO_2 crustal gases and fractionation between water and gas phases in either open or closed system. Helium isotopic signature is a particular strength for source identification in CO_2 spring samples because it can be corrected for atmospheric component. In contrast, neon and argon isotope ratios are likely to be close to the values of air.

A useful way to think about the addition of radiogenic ^4He by addition of non-CO_2 radiogenic component is to model it as a function of either time or distance. The ^4He dating approach presented here allows constraint of the residence time needed to accumulate ^4He and use this to discriminate between alternative interpretations based on their feasibility in the geological context. While a more comprehensive modelling technique might be needed if an accurate age is the objective of the study (Zhou and Ballentine, 2006; Liu et al., 2016), this method confirmed in-situ ^4He accumulation as a viable process in the studied well gases but not in CO_2 springs. The spatial distribution of $^3He/^4He$ ratios in the springs indicated that the distance from the main conduit is a more important factor in CO_2 springs. This is controlled by the interaction with ^4He-enriched stagnant basement fluids and can be modelled as fluid dispersion or a solubility process, depending if CO_2 is assumed to migrate dissolved in water or in a gas phase. In case of the former, our data are in good agreement with similar observations in volcanic settings (Sano et al., 1990). The latter is also viable and would produce a similar pattern.

Radiogenic ^4He can also be added by mixing with a crustal CO_2 source. In this case, decreasing $^3He/^4He$ ratios should correlate with an increase in $CO_2/^3He$ and either a negative or positive shift in $\delta^{13}C(CO_2)$ values, following a trajectory of mixing lines. Alternatively, it is possible that ^4He addition is decoupled from a secondary phase separation process controlling $\delta^{13}C(CO_2)$ values and $CO_2/^3He$ ratios. In this case, no clear correlation between and $CO_2/^3He$ and $^3He/^4He$ is expected. If the system is characterised by progressive gas loss in an open system, generally a significant progressive enrichment of $\delta^{13}C(CO_2)$ values is expected in non-geothermal temperatures.

Alternatively, the sample suite may effectively represent a series of individual systems, where water and gas equilibrate under different gas/water ratios. In this case, no particular trend is anticipated. The variation of $\delta^{13}C(CO_2)$ values can instead be controlled by the phase separation at different pH and temperature conditions. Temperature and pH readings of waters should always be taken to account for this effect. All noble and major gas concentrations and their relative ratios, including $CO_2/^3He$ are modified by dissolution in water and/or degassing, while elemental ratios are not expected to change. This can be tested by modelling fractionation under different gas/water ratios, which should be consistent across all element pairs. Importantly, we show how solubility models can be tested by incorporating Ne, Ar, Kr and Xe concentration data, which are often not interpreted in natural spring studies because of the air-like isotopic ratios. While $CO_2/^3He$ is expected to be easily modified, $^3He/^4He$ ratio is not altered by phase partitioning and is a reliable indicator of gas provenance.

5. Conclusions

$^3He/^4He$ and $CO_2/^3He$ ratios in well gas and CO_2 spring samples in the Otway Basin and the Central Victorian Highlands show unambiguous evidence for a predominantly mantle origin for the CO_2 stored in the gas fields and actively migrating to the surface at the springs. The main processes modifying noble gas geochemical signatures are crustal ^4He addition and noble gas elemental fractionation between the water and gas phases.

$^3He/^4He$ ratios in well gases vary due to mixing with methane, which has crustal helium contents directly dependent on gas residence time in the reservoir. The $^3He/^4He$ ratio variation in CO_2 springs is controlled by interaction with ^4He-enriched basement pore fluids and is directly dependent on the radial distance to the gas supply conduit. The observed decline in $^3He/^4He$ ratios with distance suggests that CO_2 is supplied from a single conduit in the area around Argyle spring. $^3He/^4He$ ratios are the highest in samples clustered near the Muckleford Fault and smaller parallel faults in its vicinity, suggesting that one of these basement lineaments could be acting as a pathway for mantle CO_2 to reach the shallow subsurface.

The variability of noble gas abundance patterns observed in the CO_2 springs can be explained by solubility fractionation during equilibration with groundwater. If gas is dissolved in water, transported and exsolved at the surface, a two-step dissolution and degassing process can be considered. If gases ascend to the surface dissolved in water, original $CO_2/^3He$ ratios are unlikely to be preserved. In CVH springs, $CO_2/^3He$ ratios in the range of $10^{11} – 10^{12}$ correlate with decreasing

concentrations of all noble gases and can be explained by variation of gas/water ratios during dissolution in water. Gas/water ratios up to 1 during the dissolution stage can explain the maximum observed fractionation in $CO_2/^3He$ ratios. The $\delta^{13}C(CO_2)$ values are controlled by dissolution and degassing at pH range of 5.8 - 6.3. This internally consistent model explains the abundance and isotopic signature in He, Ne, Ar, Kr, Xe and $\delta^{13}C(CO_2)$.

Taking these processes into account, noble gas compositions observed in well gases in Port Campbell, Mount Gambier, as well as CO_2 springs in CVH and Clifton Springs are traced back to a single end member of $^3He/^4He$ of 3.07 - 3.65 R_A, proving a common source. This implies a uniform regional gas composition in the Otway basin and CVH.

Importantly, we present evidence that ^3He loss resulting in high $CO_2/^3He$ ratios, commonly associated with crustal CO_2 addition, can be explained without the need to invoke mixing with crustal CO_2, which is especially important in the absence of a clear mixing trend in $\delta^{13}C(CO_2)$ values. Hence, $CO_2/^3He$ values should be compared to the concentrations of other noble gases and used with caution when assessing the origin of CO_2 degassing at surface springs.

The techniques outlined in this paper can be used to identify the origin of CO_2 seeps at the surface and their connectivity to reservoir gases. Hence, they can be applied to CO_2 sequestration or other industrial fugitive gas monitoring settings, such as surrounding shale gas operations. Helium-CO_2 abundance relationship can be used to determine the gas connectivity as long as the industrial gas has a different initial He isotope ratio to the ASW end-member. The genetic link between separate CO_2 seeps can be tested by applying solubility fractionation modelling to account for changes in noble gas concentrations caused by interaction with water. Noble gases are particularly sensitive tracers to small-scale gas migration and should be considered for surface monitoring of any industrial site where emission of fugitive gas is possible.

Acknowledgments

This work was supported by an EPSRC PhD studentship in partnership with CO2CRC and Badley Geoscience Ltd. G. Johnson and S. Gilfillan were partially supported by both UKCCSRC and Scottish Carbon Capture and Storage (SCCS), S. Serno was funded by the UK Carbon Capture and Storage Research Centre (UKCCSRC) Call 2 grant. S. Flude was supported by by EPSRC grant #EP/K036033/1. We thank the field operators – BOC, Air Liquide and CO2CRC for permission to sample the gas reservoirs. Craig Vivian and Peter Dumsey are thanked for support while sampling in the field. We thank Terry Donnelly and Marta Zurakowska at SUERC for assistance in obtaining stable

763 isotope and noble gas measurements of gas samples. Ian Cartwright is thanked for providing
764 background data on the Daylesford springs.

765

References

Aeschbach-Hertig W., El-Gamal H., Wieser M. and Palcsu L. (2008) Modeling excess air and degassing in groundwater by equilibrium partitioning with a gas phase. *Water Resour. Res.* **44**, 1–12.

Aka F. T., Kusakabe M., Nagao K. and Tanyileke G. (2001) Noble gas isotopic compositions and water/gas chemistry of soda springs from the islands of Bioko, São Tomé and Annobon, along with Cameroon Volcanic Line, West Africa. *Appl. Geochemistry* **16**, 323–338.

Akbari V. (1992) *Boggy Creek No.1 Well Completion Report*., Available at: http://geoscience-web.s3-website-ap-southeast-2.amazonaws.com/well/boggycreek1.htm.

Baines S. J. and Worden R. H. (2004) The long term fate of CO_2 in the subsurface: natural analogues for CO_2 storage. In *Geological Storage of Carbon Dioxide* (ed. R. H. Baines, S.J., Worden). Geological Society, London. pp. 59–85.

Ballentine C. J. and Burnard P. G. (2002) Production, Release and Transport of Noble Gases in the Continental Crust. *Rev. Mineral. Geochemistry* **47**, 481–538.

Ballentine C. J. and O'Nions R. K. (1994) The use of natural He, Ne and Ar isotopes to study hydrocarbon-related fluid provenance, migration and mass balance in sedimentary basins. *Geol. Soc. London, Spec. Publ.* **78**, 347–361.

Ballentine C. J., O'Nions R. K. and Coleman M. L. (1996) A Magnus opus: Helium, neon, and argon isotopes in a North Sea oilfield. *Geochim. Cosmochim. Acta* **60**, 831–848.

Barry P. H., Lawson M., Meurer W. P., Warr O., Mabry J. C., Byrne D. J. and Ballentine C. J. (2016) Noble gases solubility models of hydrocarbon charge mechanism in the Sleipner Vest gas field. *Geochim. Cosmochim. Acta* **194**, 291–309.

Bernecker T. and Moore D. H. H. (2003) Linking basement and basin fill: implications for hydrocarbon prospectivity in the Otway Basin Region. *APPEA J.* **43**, 39–58.

Boreham C. J., Hope J. M., Jackson P., Davenport R., Earl K. L., Edwards D. S., Logan G. A. and Krassay A. A. (2004) Gas – oil – source correlations in the Otway Basin, southern Australia. In Petroleum Exploration Society of Australia (PESA). pp. 19–22.

Boreham C., Underschultz J., Stalker L., Kirste D., Freifeld B., Jenkins C. and Ennis-King J. (2011) Monitoring of CO_2 storage in a depleted natural gas reservoir: Gas geochemistry from the CO_2CRC Otway Project, Australia. *Int. J. Greenh. Gas Control* **5**, 1039–1054.

795 Bosch A. and Mazor E. (1988) Natural gas association with water and oil as depicted by atmospheric
796 noble gases: case studies from the southeastern Mediterranean Coastal Plain. *Earth Planet. Sci.*
797 *Lett.* **87**, 338–346.

798 Bottomley D. ., Ross J. . and Clarke W. . (1984) Helium and neon isotope geochemistry of some
799 ground waters from the Canadian Precambrian Shield. *Geochim. Cosmochim. Acta* **48**, 1973–
800 1985.

801 Boult P. J., Johns D. R. and Lang S. C. (2004) Subsurface plumbing of the Crayfish Group in the Penola
802 Trough: Otway Basin. In *Eastern Australasian Basins Symposium II* Petroleum Exploration
803 Society of Australia (PESA). pp. 483–498.

804 Boyce J. (2013) The Newer Volcanics Province of southeastern Australia: a new classification scheme
805 and distribution map for eruption centres. *Aust. J. Earth Sci.* **60**, 449–462.

806 Bräuer K., Geissler W. H., Kämpf H., Niedermannn S. and Rman N. (2016) Helium and carbon isotope
807 signatures of gas exhalations in the westernmost part of the Pannonian Basin (SE Austria/NE
808 Slovenia): Evidence for active lithospheric mantle degassing. *Chem. Geol.* **422**, 60–70.

809 Caffee, M.W., Hudson, G.B., Velsko, C., Huss, G.R., Alexander, E.C. and Chivas A. R. (1999) Primordial
810 Noble Gases from Earth's Mantle: Identification of a Primitive Volatile Component. *Science.*
811 **285**, 2115–2118.

812 Cartwright I., Weaver T., Tweed S., Ahearne D., Cooper M., Czapnik K. and Tranter J. (2002) Stable
813 isotope geochemistry of cold CO_2-bearing mineral spring waters, Daylesford, Victoria, Australia:
814 Sources of gas and water and links with waning volcanism. *Chem. Geol.* **185**, 71–91.

815 Cas R. A. F., van Otterloo J., Blaikie T. N. and van den Hove J. (2017) The dynamics of a very large
816 intra-plate continental basaltic volcanic province, the Newer Volcanics Province, SE Australia,
817 and implications for other provinces. *Geol. Soc. London, Spec. Publ.* **446**, 123–172.

818 Cayley R. A., Korsch R. J., Moore D. H., Costelloe R. D., Nakamura A., Willman C. E., Rawling T. J.,
819 Morand V. J., Skladzien P. B. and O'Shea P. J. (2011) Crustal architecture of central Victoria:
820 Results from the 2006 deep crustal reflection seismic survey. *Aust. J. Earth Sci.* **58**, 113–156.

821 Chivas A. R., Barnes I. E., Lupton J. E. and Collerson K. (1983) Isotopic studies of south-east Australian
822 CO_2 discharges. *Geol. Soc. Aust. Abstr.* **12**, 94–95.

823 Chivas A. R., Barnes I., Evans W. C., Lupton J. E. and Stone J. O. (1987) Liquid carbon dioxide of
824 magmatic origin and its role in volcanic eruptions. *Nature* **326**, 587–589.

825 Clennell M. Ben (1997) Tortuosity: a guide through the maze. *Geol. Soc. London, Spec. Publ.* **122**,
826 299–344.

827 Coulson A. (1933) The older volcanic and Tertiary marine beds at Curlewis, near Geelong. *Proc. R.*
828 *Soc. Victoria* **45**, 140–149.

829 Cox S. F., Sun S. S., Etheridge M. A., Wall V. J. and Potter T. F. (1995) Structural and geochemical
830 controls on the development of turbidite- hosted gold quartz vein deposits, Wattle Gully mine,
831 central Victoria, Australia. *Econ. Geol.* **90**, 1722–1746.

832 Craig H. (1978) A mantle helium component in circum-Pacific volcanic gases: Hakone, the Marianas
833 and Mt. Lassen. *Terriestrial Rare Gases*, 3–16.

834 Craig H. and Lupton J. E. (1976) Primordial neon, helium, and hydrogen in oceanic basalts. *Earth*
835 *Planet. Sci. Lett.* **31**, 369–385.

836 Crossey L. J., Karlstrom K. E., Springer A. E., Newell D., Hilton D. R. and Fischer T. (2009) Degassing of
837 mantle-derived CO_2 and He from springs in the southern Colorado Plateau region - Neotectonic
838 connections and implications for groundwater systems. *Bull. Geol. Soc. Am.* **121**, 1034–1053.

839 Crovetto R. (1991) Evaluation of solubility data of the system CO_2–H_2O from 273 K to the critical
840 point of water. *J. Phys. Chem. Ref. Data* **20**, 575–589.

841 Crovetto R., Fernández-Prini R. and Japas M. L. (1982) Solubilities of inert gases and methane in H_2O
842 and in D_2O in the temperature range of 300 to 600 K. *J. Chem. Phys.* **76**, 1077–1086.

843 Dahlhaus (2003) *The Dell, Clifton Springs. 3-dimensional geological model*., Available at:
844 http://www.ccmaknowledgebase.vic.gov.au/soilhealth/soils_resource_details.php?resource_id
845 =2416.

846 Darrah T. H., Vengosh A., Jackson R. B., Warner N. R. and Poreda R. J. (2014) Noble gases identify the
847 mechanisms of fugitive gas contamination in drinking-water wells overlying the Marcellus and
848 Barnett Shales. *Proc. Natl. Acad. Sci.* **111**, 14076–14081.

849 Davies D. R. and Rawlinson N. (2014) On the origin of recent intraplate volcanism in Australia.
850 *Geology* **42**, 1031–1034.

851 Deines P., Langmuir D. and Harmon R. S. (1974) Stable carbon isotope ratios and the existence of a
852 gas phase in the evolution of carbonate ground waters. *Geochim. Cosmochim. Acta* **38**, 1147–
853 1164.

Demidjuk Z., Turner S., Sandiford M., George R., Foden J. and Etheridge M. (2007) U-series isotope and geodynamic constraints on mantle melting processes beneath the Newer Volcanic Province in South Australia. *Earth Planet. Sci. Lett.* **261**, 517–533.

Dixon T., McCoy S. T. and Havercroft I. (2015) Legal and regulatory developments on CCS. *Int. J. Greenh. Gas Control* **40**, 431–448.

Duddy I. R. (1997) Focussing exploration in the Otway Basin: understanding timing of source rock maturation. *APPEA J.* **37**, 178–191.

Dunbar E., Cook G. T., Naysmith P., Tripney B. G. and Xu S. (2016) AMS ^{14}C dating at the Scottish Universities Environmental Research Centre (SUERC) radiocarbon dating laboratory. *Radiocarbon* **58**, 9–23.

Eberhardt P., Eugster O. and Marti K. (1965) A redetermination of the isotopic composition of atmospheric neon. *Zeitschrift für Naturforsch. A* **20**, 623–624.

Giese R., Henninges J., Lüth S., Morozova D., Schmidt-Hattenberger C., Würdemann H., Zimmer M., Cosma C. and Juhlin C. (2009) Monitoring at the CO_2 SINK site: A concept integrating geophysics, geochemistry and microbiology. *Energy Procedia* **1**, 2251–2259.

Giggenbach W. F., Sano Y. and Wakita H. (1993) Isotopic composition of helium, and CO_2 and CH_4 contents in gases produced along the New Zealand part of a convergent plate boundary. *Geochim. Cosmochim. Acta* **57**, 3427–3455.

Gilfillan S., Haszedline S., Stuart F., Gyore D., Kilgallon R. and Wilkinson M. (2014) The application of noble gases and carbon stable isotopes in tracing the fate, migration and storage of CO_2. *Energy Procedia* **63**, 4123–4133.

Gilfillan S. M. V., Sherk G. W., Poreda R. J. and Haszeldine R. S. (2017) Using noble gas fingerprints at the Kerr Farm to assess CO_2 leakage allegations linked to the Weyburn-Midale CO_2 monitoring and storage project. *Int. J. Greenh. Gas Control* **63**, 215–225.

Gilfillan S. M. V, Ballentine C. J., Holland G., Blagburn D., Lollar B. S., Stevens S., Schoell M. and Cassidy M. (2008) The noble gas geochemistry of natural CO_2 gas reservoirs from the Colorado Plateau and Rocky Mountain provinces, USA. *Geochim. Cosmochim. Acta* **72**, 1174–1198.

Gilfillan S. M. V, Lollar B. S., Holland G., Blagburn D., Stevens S., Schoell M., Cassidy M., Ding Z., Zhou Z., Lacrampe-Couloume G. and Ballentine C. J. (2009) Solubility trapping in formation water as dominant CO(2) sink in natural gas fields. *Nature* **458**, 614–618.

884 Györe D., Gilfillan S. M. V. and Stuart F. M. (2017) Tracking the interaction between injected CO_2 and
885 reservoir fluids using noble gas isotopes in an analogue of large-scale carbon capture and
886 storage. *Appl. Geochemistry* **78**, 116–128.

887 Györe D., Stuart F. M., Gilfillan S. M. V and Waldron S. (2015) Tracing injected CO_2 in the Cranfield
888 enhanced oil recovery field (MS, USA) using He, Ne and Ar isotopes. *Int. J. Greenh. Gas Control*
889 **42**, 554–561.

890 Hand M. and Sandiford M. (1999) Intraplate deformation in central Australia, the link between
891 subsidence and fault reactivation. *Tectonophysics* **305**, 121–140.

892 Haszeldine R. S., Quinn O., England G., Wilkinson M., Shipton Z. K., Evans J. P., Heath J., Crossey L.,
893 Ballentine C. J. and Graham C. M. (2005) Natural geochemical analogues for carbon dioxide
894 storage in deep geological porous reservoirs, a United Kingdom perspective. *Oil Gas Sci.*
895 *Technol.* **60**, 33–49.

896 Hilton D. R. (2009) The helium and carbon isotope systematics of a continental geothermal system:
897 results from monitoring studies at Long Valley caldera (California, U.S.A.). **127**, 1–27.

898 Holland G. and Gilfillan S. (2013) Application of noble gases to the viability of CO_2 storage. In *The*
899 *Noble Gases as Geochemical Tracers,* Springer Berlin Heidelberg, Berlin, Heidelberg. pp. 177–
900 223.

901 Holland G., Lollar B. S., Li L., Lacrampe-Couloume G., Slater G. F. and Ballentine C. J. (2013) Deep
902 fracture fluids isolated in the crust since the Precambrian era. *Nature* **497**, 357–360.

903 IPCC (2005) *IPCC Special Report on Carbon Dioxide Capture and Storage*., UK: Cambridge University
904 Press, New York. Available at: https://www.ipcc.ch/pdf/special-
905 reports/srccs/srccs_wholereport.pdf.

906 Italiano F., Yuce G., Uysal I. T., Gasparon M. and Morelli G. (2014) Insights into mantle-type volatiles
907 contribution from dissolved gases in artesian waters of the Great Artesian Basin, Australia.
908 *Chem. Geol.* **378**–**379**, 75–88.

909 Jeandel E., Battani A. and Sarda P. (2010) Lessons learned from natural and industrial analogues for
910 storage of carbon dioxide. *Int. J. Greenh. Gas Control* **4**, 890–909.

911 Karolytė R., Serno S., Johnson G. and Gilfillan S. M. V. (2017) The influence of oxygen isotope
912 exchange between CO_2 and H_2O in natural CO_2-rich spring waters: Implications for
913 geothermometry. *Appl. Geochemistry* **84**, 173–186.

King S. D. and Anderson D. L. (1998) Edge-driven convection. *Earth Planet. Sci. Lett.* **160**, 289–296.

Kipfer R., Aeschbach-Hertig W., Peeters F. and Stute M. 4 Noble Gases in Lakes and Ground Waters.

Kipfer R., Aeschbach-Hertig W., Peeters F. and Stute M. (2002) Noble Gases in Lakes and Ground Waters. *Rev. Mineral. Geochemistry* **47**, 615–700.

Lawrence C. R. (1969) Hydrogeology of the Daylesford Mineral District with special reference to the mineral springs. *Geol. Surv. Victoria, Undergr. water Investig. Rep.* **12**.

Lee J.-Y., Marti K., Severinghaus J. P., Kawamura K., Yoo H.-S., Lee J. B. and Kim J. S. (2006) A redetermination of the isotopic abundances of atmospheric Ar. *Geochim. Cosmochim. Acta* **70**, 4507–4512.

Lesti C., Giordano G., Salvini F. and Cas R. (2008) Volcano tectonic setting of the intraplate, Pliocene-Holocene, Newer Volcanic Province (southeast Australia): Role of crustal fracture zones. *J. Geophys. Res. Solid Earth* **113**, 1–11.

Liu W., Tao C., Borjigin T., Wang J., Yang H., Wang P., Luo H. and Zhai C. (2016) Formation time of gas reservoir constrained by the time-accumulation effect of 4He: Case study of the Puguang gas reservoir. *Chem. Geol.* **469**, 246–251.

Lyon P. J., Boult P. J., Watson M. N. and Hillis R. (2005) A systematic fault seal evaluation of the Ladbroke Grove and Pyrus traps of the Penold Trough, Otway Basin. *Aust. Pet. Prod. Explor. Assoc. J.* **45**, 459–476.

Mao X., Wang Y., Chudaev O. V. and Wang X. (2009) Geochemical evidence of gas sources of CO_2-rich cold springs from Wudalianchi, Northeast China. *J. Earth Sci.* **20**, 959–970.

Marty B. and Jambon A. (1987) C^3He in volatile fluxes from the solid Earth: implications for carbon geodynamics. *Earth Planet. Sci. Lett.* **83**, 16–26.

Marty B. and Tolstikhin I. N. (1998) CO_2 fluxes from mid-ocean ridges, arcs and plumes. *Chem. Geol.* **145**, 233–248.

Matsumoto T., Honda M., Mcdougall I. and O'reilly S. Y. (1998) Noble gases in anhydrous lherzolites from the Newer Volcanics, southeastern Australia: A MORB-like reservoir in the subcontinental mantle.

Matsumoto T., Honda M., McDougall I., Yatsevich I. and O'reilly S. Y. (1997) Plume-like neon in a metasomatic apatite from the Australian lithospheric mantle. Nature 388, 162.

943 Matsumoto T., Pinti D. L., Matsuda J. and Umino S. (2002) Recycled noble gas and nitrogen in the
944 subcontinental lithospheric mantle: Implications from N-He-Ar in fluid inclusions of SE
945 Australian xenoliths. Geochem. J. 36, 209–217.

946 Matthews A., Fouillac C., Hill R., O'Nions R. K. and Oxburgh E. R. (1987) Mantle-derived volatiles in
947 continental crust: the Massif Central of France. *Earth Planet. Sci. Lett.* **85**, 117–128.

948 Myers M., Stalker L., Pejcic B. and Ross A. (2013) Tracers – Past, present and future applications in
949 CO_2 geosequestration. *Appl. Geochemistry* **30**, 125–135.

950 Newell D. L., Jessup M. J., Hilton D. R., Shaw C. A. and Hughes C. A. (2015) Mantle-derived helium in
951 hot springs of the Cordillera Blanca, Peru: Implications for mantle-to-crust fluid transfer in a
952 flat-slab subduction setting. *Chem. Geol.* **417**, 200–209.

953 O'Nions R. K. and Oxburgh E. R. (1988) Helium, volatile fluxes and the development of continental
954 crust. *Earth Planet. Sci. Lett.* **90**, 331–347.

955 Ozima M. and Podosek F. A. (2002) *Noble Gas Geochemistry*., Cambridge University Press.

956 Price R. C., Gray C. M. and Frey F. A. (1997) Strontium isotopic and trace element heterogeneity in
957 the plains basalts of the Newer Volcanic Province, Victoria, Australia. *Geochim. Cosmochim.*
958 *Acta* **61**, 171–192.

959 Roberts J. J., Gilfillan S. M. V., Stalker L. and Naylor M. (2017) Geochemical tracers for monitoring
960 offshore CO_2 stores. *Int. J. Greenh. Gas Control* **65**, 218–234.

961 Roberts J. J., Leplastrier A., Feitz A. J., Shipton Z. K., Bell A. F. and Karolytė R. (2019) Structural
962 controls on the location and distribution of CO_2 emission at a natural CO_2 spring in Daylesford,
963 Australia. *Int. J. Greenh. Gas Control* **84**, 36–46.

964 Robertson G. B., Prescott J. R. and Hutton J. T. (1996) Thermoluminescence dating of volcanic activity
965 at Mount Gambier, South Australia. *Trans. R. Soc. South Aust.* **120**, 7–12.

966 Rudnick R. L. and Fountain D. M. (1995) Nature and composition of the continental crust: A lower-
967 crustal perspective. *Rev. Geophys.* **33**, 267–309.

968 Ruzié L., Aubaud C., Moreira M., Agrinier P., Dessert C., Gréau C. and Crispi O. (2013) Carbon and
969 helium isotopes in thermal springs of La Soufrière volcano (Guadeloupe, Lesser Antilles):
970 Implications for volcanological monitoring. *Chem. Geol.* **359**, 70–80.

971 Sakamoto M., Sano Y. and Wakita H. (1992) $^3He/^4He$ ratio distribution in and around the Hakone

volcano. *Geochem. J.* **26**, 189–195.

Sano Y. and Marty B. (1995) Origin of carbon in fumarolic gas from island arcs. *Chem. Geol.* **119**, 265–274.

Sano Y., Takahata N. and Seno T. (2006) Geographical distribution of $^{3}He/^{4}He$ ratios in the Chugoku District, Southwestern Japan. *Pure Appl. Geophys.* **163**, 745–757.

Sano Y., Wakita H. and Williams S. N. (1990) Helium-isotope systematics at Nevado del Ruiz volcano, Colombia: implications for the volcanic hydrothermal system. *J. Volcanol. Geotherm. Res.* **42**, 41–52.

Sherwood Lollar B., Ballentine C. J. and O'Nions R. K. (1997) The fate of mantle-derived carbon in a continental sedimentary basin: Integration of relationships and stable isotope signatures. *Geochim. Cosmochim. Acta* **61**, 2295–2307.

Sherwood Lollar B., O'Nions R. K. and Ballentine C. J. (1994) Helium and neon isotope systematics in carbon dioxide-rich and hydrocarbon-rich gas reservoirs. *Geochim. Cosmochim. Acta* **58**, 5279–5290.

Shugg A. (2009) Hepburn Spa: Cold carbonated mineral waters of Central Victoria, South Eastern Australia. *Environ. Geol.* **58**, 1663–1673.

Smith S. P. (1985) Noble gas solubility in water at high temperature. *Eos (Washington. DC).* **66**, 397.

Stalker L. and Myers M. (2014) Tracers–pilot versus commercial scale deployment for carbon storage. *Energy Procedia* **63**, 4199–4208.

Teasdale J. P., Pryer L. L., Stuart-Smith P. G., Romine K. K., Etheridge M. A., Loutit T. S. and Kyan D. M. (2003) Structural framework and basin evolution of Australia's southern margin. *APPEA J.* **43**, 13–37.

Tolstikhin I. N., Ballentine C. J., Polyak B. G., Prasolov E. M. and Kikvadze O. E. (2017) The noble gas isotope record of hydrocarbon field formation time scales. *Chem. Geol.* **471**, 141–152.

Torgersen T. (1980) Controls on pore-fluid concentration of ^{4}He and ^{222}Rn and the calculation of $^{4}He/^{222}Rn$ ages. *J. Geochemical Explor.* **13**, 57–75.

van Otterloo J., Cas R. A. F. and Sheard M. J. (2013) Eruption processes and deposit characteristics at the monogenetic Mt. Gambier Volcanic Complex, SE Australia: implications for alternating magmatic and phreatomagmatic activity. *Bull. Volcanol.* **75**, 737.

van Otterloo J., Raveggi M., Cas R. A. F. and Maas R. (2014) Polymagmatic activity at the monogenetic Mt Gambier Volcanic Complex in the Newer Volcanics Province, SE Australia: New insights into the occurrence of intraplate volcanic activity in Australia. *J. Petrol.* **55**, 1317–1351.

Walton N. R. G. (1989) Electrical conductivity and Total Dissolved Solids—what is their precise relationship? *Desalination* **72**, 275–292.

Warr O., Sherwood Lollar B., Fellowes J., Sutcliffe C. N., McDermott J. M., Holland G., Mabry J. C. and Ballentine C. J. (2018) Tracing ancient hydrogeological fracture network age and compartmentalisation using noble gases. *Geochim. Cosmochim. Acta* **222**, 340–362.

Watson M. N., Boreham C. J. and Tingate P. R. (2004) Carbon dioxide and carbonate cements in the Otway Basin; implications for geological storage of carbon dioxide. *APPEA J.* **44**, 703–720.

Watson M. N., Zwingmann N., Lemon N. M. and Tingate P. R. (2003) Onshore Otway Basin carbon dioxide accumulations: CO_2-induced diagenesis in natural analogues for underground storage of greenhouse gas. *APPEA J.* **43**, 637–653.

Weast R. C., Astle M. J. and Beyer W. H. (1988) *CRC Handbook of Chemistry and Physics*., CRC press Boca Raton, FL.

Weinlich F. H., Bräuer K., Kämpf H., Strauch G., Tesař J. and Weise S. M. (1999) An active subcontinental mantle volatile system in the western Eger rift, Central Europe: Gas flux, isotopic (He, C, and N) and compositional fingerprints. *Geochim. Cosmochim. Acta* **63**, 3653–3671.

Wellman P. (1983) Hotspot volcanism in Australia and New Zealand: Cainozoic and mid-Mesozoic. *Tectonophysics* **96**, 225–243.

Wellman P. and McDougall I. (1974) Cainozoic igneous activity in eastern Australia. *Tectonophysics* **23**, 49–65.

Wilkinson M., Gilfillan S. M. V, Haszeldine R. S. and Ballentine C. J. (2009) Plumbing the Depths: Testing Natural Tracers of Subsurface CO_2 Origin and Migration, Utah. In *Carbon dioxide sequestration in geological media-State of the science* AAPG Special Volumes. pp. 619–634.

Williams S. N., Sano Y. and Wakita H. (1987) Helium-3 emission from Nevado Del Ruiz Volcano, Colombia. *Geophys. Res. Lett.* **14**, 1035–1038.

Wycherley H., Fleet A. and Shaw H. (1999) Some observations on the origins of large volumes of

carbon dioxide accumulations in sedimentary basins. *Mar. Pet. Geol.* **16**, 489–494.

Zartman R. E., Wasserburg G. J. and Reynolds J. H. (1961) Helium, argon, and carbon in some natural gases. *J. Geophys. Res.* **66**, 277–306.

Zhou Z. and Ballentine C. J. (2006) ^{4}He dating of groundwater associated with hydrocarbon reservoirs. *Chem. Geol.* **226**, 309–327.